



1 **Effects of 20-100 nanometre particles on liquid clouds in the clean**
2 **summertime Arctic**

3

4 W. R. Leaitch, A. Korolev, A. A. Aliabadi

5 Environment Canada, Toronto, Canada

6

7 J. Burkart, M. Willis, J.P.D. Abbatt

8 Department of Chemistry, University of Toronto, Toronto, Canada

9

10 H. Bozem, P. Hoor

11 Institute of Atmospheric Physics, University of Mainz, Mainz, Germany

12

13 F. Köllner, J. Schneider

14 Particle Chemistry Department, Max Planck Institute for Chemistry, Mainz, Germany

15

16 A. Herber, C. Konrad

17 Alfred Wegener Institute for Polar and Marine Research, Bremerhaven, Germany

18

19 R. Brauner

20 Jade University, Elsfleth, Germany

21

22 Date: January 27, 2016

23

24 Correspondence to Richard.Leaitch@Canada.ca

25

26



27 **Abstract.** Aerosol-cloud research in the Arctic has largely focused on the springtime resulting
28 in relatively little information about the effects of the atmospheric aerosol on Arctic clouds
29 during summer. An airborne study, carried out during July, 2014 from Resolute Bay, Nunavut,
30 Canada, provides a comprehensive in-situ look into some effects of aerosol particles on liquid
31 clouds in the clean environment of the Arctic summer. The median cloud droplet number
32 concentrations (CDNC) are 10 cm^{-3} and 101 cm^{-3} for low altitude cloud (LA: clouds topped
33 below 200 m) and higher altitude cloud (HA: clouds based above 200 m), respectively. The
34 mean lower activation size of aerosol particles is $\leq 50\text{ nm}$ diameter in 40% of the cases, and
35 particles as small as 20 nm activated in the HA clouds consistent with the higher supersaturations
36 inferred for those clouds. Over 60% of the LA cloud cases fall into the cloud condensation nuclei
37 (CCN)-limited regime of Mauritsen et al. (2011) within which increases in CDNC may increase
38 liquid water and warm the surface. In that CCN-limited regime, the liquid water contents (LWC)
39 and the CDNC are positively correlated, but there is no dependence of changes in either the
40 CDNC or LWC on the aerosol, suggesting no aerosol limitation. Above the Mauritsen limit,
41 where indirect cooling may result, particles with diameters from 20 nm to 100 nm exert a strong
42 influence on the CDNC. Based on CO concentrations, the background CDNC are estimated to
43 range between 16 cm^{-3} and 160 cm^{-3} , implying a large uncertainty for the baseline of the aerosol
44 cloud albedo effect.

45



46 1. Introduction

47

48 Mass concentrations of the atmospheric aerosol in the Arctic are higher during winter and lower
49 during summer due to differences in the transport of the anthropogenic aerosol and wet
50 scavenging (e.g. Barrie, 1986; Stohl, 2006). Much of the focus of atmospheric chemistry and
51 aerosol-cloud research in the Arctic has been on the spring period. The transition from winter to
52 summer offers the opportunity to examine the changes in chemistry as the sun rises over the
53 polluted polar atmosphere (e.g. Barrie et al., 1988) and to study the impacts of the anthropogenic
54 aerosol on the Arctic solar radiation balance (e.g. Law and Stohl, 2007; Quinn et al., 2008).
55 Greater-than-expected warming of the Arctic (e.g. Christensen et al., 2013) and rapidly
56 diminishing Arctic sea ice extent (e.g. Maslanik et al., 2011) have drawn considerable attention
57 to the role of anthropogenic and biomass burning aerosols as warming agents for the Arctic (e.g.
58 Law and Stohl, 2007; Quinn et al., 2008; Shindell et al., 2008; Brock et al., 2011; Jacob et al.,
59 2010; UNEP, 2011; Stohl et al., 2013). Recent evidence indicates that the net impact of the
60 aerosol on the Arctic over the past century has been one of cooling rather than warming (Najafi
61 et al., 2015).

62 Low-level liquid water clouds are frequent in the sunlit Arctic summer (e.g. Intrieri et al.,
63 2001), and these clouds can have a net cooling effect (e.g. Brenner et al., 2001; Garret et al.,
64 2004; Lubin and Vogelmann, 2010; Zhao and Garrett, 2015; Zamora et al., 2015;). Knowledge
65 of the influence of the atmospheric aerosol on climatic aspects of these clouds is complicated by
66 the relatively large potential differences in the albedo of the underlying surface (e.g. Herman,
67 1977; Lubin and Vogelmann, 2010) and the fact that the Arctic is relatively free of
68 anthropogenic influence in the summer, which means that aerosols from natural sources can be



69 the most significant sources of nuclei for cloud droplets. Those sources shift the number
70 distribution towards particles smaller than 100 nm (e.g. Ström et al., 2003; Engvall et al., 2008;
71 Tunved et al., 2013; Leaitch et al., 2013; Browse et al., 2014; Heintzenberg et al., 2015).
72 Particles much smaller than 100 nm are sometimes dismissed as being too small to nucleate
73 cloud droplets due to the assumption that the cooling mechanisms are too slow to generate the
74 supersaturations required to activate the smaller particles in Arctic liquid clouds (e.g. Garret et
75 al., 2004; Zhao and Garrett, 2015). However, the cloud supersaturation is also constrained by the
76 concentration of the particles larger than 100 nm. In situations with few larger particles, as in the
77 clean environment of the summertime Arctic, higher supersaturations can be achieved and
78 smaller particles may be activated (e.g. Leaitch et al., 2013). Garrett et al. (2004) showed no
79 correlation of CDNC retrieved from remote sensing with surface-based total particle number
80 concentrations larger than about 10 nm, but total number concentration measurements do not
81 reflect the size distribution and the concentrations of such particles may change significantly
82 with altitude. Lubin and Vogelmann (2010) estimated substantial aerosol indirect forcings for
83 low-level spring-summer Arctic clouds based on a “natural background range” of surface-based
84 total particle number concentrations of 0-50 cm⁻³, which significantly underestimates the
85 potential contributions from natural sources as discussed in the above references. The effect of
86 the background aerosol on liquid clouds has been identified as one of the most important factors
87 for reducing uncertainty in the aerosol cloud albedo effect (Carslaw et al., 2013). A related and
88 important question is how effective are particles smaller than 100 nm at nucleating cloud
89 droplets?

90 Aerosol effects on clouds may also lead to warming, but a contrast between clean versus
91 polluted clouds is still required (e.g. Garrett et al., 2009). Mauritsen et al. (2011) modeled cloud



92 radiative forcing for low clouds using CCN number concentrations (hereafter CCNC) derived
93 from shipborne observations made over the Arctic Ocean (Tjernström et al., 2004; Tjernström et
94 al., 2014). They found that the impact from changes in CCNC for ultra-low values ($<10\text{ cm}^{-3}$),
95 where CCNC is equivalent to the CDNC in the model, will result in a net warming due to
96 associated longwave changes, whereas for $\text{CCNC} > 10\text{ cm}^{-3}$ increases in the CCNC are estimated
97 to produce a net cooling of the atmosphere. The threshold CCNC is referred to here as the
98 "Mauritsen limit", and it is noted that the value of 10 cm^{-3} is not considered universal. In such
99 clean environments, knowledge of the natural aerosol and its influence on the microphysics of
100 summer clouds is critical to the assessment of the effects of the aerosol on the Arctic climate.

101 Past studies of Arctic aerosols and clouds have emphasized the areas of the Beaufort and
102 Chukchi Seas (e.g. Hobbs and Rango, 1998; Curry et al., 2001 and references therein; Lohmann
103 et al., 2001; Peng et al., 2002; Earle et al., 2011; Lance et al., 2011; Jouan et al., 2014; Klingebiel
104 et al., 2014). Most of those studies have focused on the spring when the aerosol is influenced by
105 anthropogenic or biomass burning aerosol. As well, there has been considerable interest in
106 mixed-phase clouds in the lower Arctic troposphere (e.g. Shupe et al., 2004; Sandvik et al., 2007;
107 Morrison et al., 2012), but a notable lack of in-situ observations of aerosols in combination with
108 liquid water clouds over the Arctic during summer. Among the studies that have considered in-
109 situ measurements of aerosols and Arctic summer clouds, Zamora et al. (2015) examined the
110 efficiency of biomass burning (BB) plumes on indirect forcing, estimating a forcing from these
111 plumes about half of the possible maximum, mostly due to the reduction in cloud-base
112 supersaturation by the higher concentration and larger particles that control water uptake. Shupe
113 et al. (2013) discussed some differences among clouds coupled to the surface versus those
114 uncoupled, but did not conduct in-situ observations of the microphysics within the cloud, and



115 vertical aerosol characterization was constrained to particles >300 nm. Hobbs and Rango (1998)
116 found that droplets in low clouds over the Beaufort Sea in June occasionally contained drops as
117 large as $35\ \mu\text{m}$ diameter. They also found that the CDNC in the cloud tops correlated
118 significantly with “aerosols” below the bases. They suggested that cloud-top entrainment did not
119 control the CDNC, although there may be times when entrainment does influence the Arctic
120 CDNC (e.g. Klingebiel et al., 2014).

121 Motivated by the limited knowledge of aerosol effects on cloud in the summer Arctic and
122 the details of particle activation, the Canadian Network on Climate and Aerosols: Addressing
123 Key Uncertainties in Remote Canadian Environments (NETCARE - [http://www.netcare-](http://www.netcare-project.ca/)
124 [project.ca/](http://www.netcare-project.ca/)), conducted airborne observations of aerosols and clouds during July, 2014 in the area
125 around Resolute Bay, Nunavut, Canada. The observations from the study are used here to
126 characterize CDNC, LWC, and the volume-weighted mean droplet diameter (VMD) relative to
127 measured aerosol particle size distributions (5 nm and larger) and CCNC. In particular, the
128 following questions are addressed:

- 129 1) Given the scarcity of data, what are the characteristics of clouds in the summertime Arctic,
130 and do clouds near the surface have characteristics different from those aloft? (Sect. 3.2)
- 131 2) What are the sizes of particles that are acting as nuclei for cloud droplets, which will allow a
132 closer connection between aerosol processes, particle sizes and climate effects? (Sect. 3.3)
- 133 3) What is the relationship between droplet size and droplet number? In particular, what is the
134 aerosol influence on cloud below the Mauritsen-limit, and is it possible to assess a
135 background influence of the aerosol on clouds in the Arctic summer? (Sect. 3.4)

136



137 **2. Methodologies**

138

139 The instrument platform was the Alfred Wegener Institute (AWI) Polar 6 aircraft, a DC-3
140 aircraft converted to a Basler BT-67 (see Herber, A., Dethloff, K., Haas, C., Steinhage, D.,
141 Strapp, J. W., Bottenheim, J., McElroy, T. and Yamanouchi, T.; POLAR 5 - a new research
142 aircraft for improved access to the Arctic, ISAR-1, Drastic Change under the Global Warming,
143 Extended Abstract, pp. 54-57, 2008).

144

145 **2.1 Instrumentation**

146

147 The following measurements are relevant to this discussion:

- 148 a) Particle number concentrations >5 nm diameter were measured with a TSI 3787 water-
149 based ultrafine condensation particle counter (UCPC), sampling at a flow rate of 0.6 L
150 min^{-1} . Hereafter, the measurements are referred to as N5.
- 151 b) Aerosol particle size distributions from 20 nm to 100 nm (45 s up scans and 15 s down
152 scans) were measured using a Brechtel Manufacturing Incorporated (BMI) Scanning
153 Mobility System (SMS) coupled with a TSI 3010 Condensation Particle Counter (CPC).
154 The sheath and sample flows were set to 6 L min^{-1} and 1 L min^{-1} . BMI software was used
155 to process the distributions.
- 156 c) Aerosol particle size distributions from 70 nm to 1 μm were measured using a Droplet
157 Measurement Technology (DMT) Ultra High Sensitivity Aerosol Spectrometer (UHSAS)
158 that uses scattering of 1054 nm laser light to detect particles (e.g. Cai et al., 2008).



- 159 d) CCNC were measured using a DMT CCN Model 100 counter operating behind a DMT
160 low pressure inlet at a reduced pressure of approximately 650 hPa. For the nominal water
161 supersaturation of 1%, the effective supersaturation at 650 hPa was found to be 0.6% as
162 discussed below. The supersaturation was held constant throughout the study to allow for
163 more stability of measurement, improved response, and to examine the hygroscopicity of
164 smaller particles.
- 165 e) Droplet size distributions from 2-45 μm were measured using a Particle Measuring
166 Systems (PMS) FSSP-100. This FSSP-100 had been modified with new tips to reduce
167 shattering artifacts (Korolev et al., 2011), and it was mounted in a canister under the port-
168 side wing. The CDNC, VMD and LWC are calculated from the measured droplet
169 distributions.
- 170 f) Cloud particle images in two dimensions for particles sized from about 50 μm to 800 μm
171 were measured using a PMS 2DC Grey-scale probe. For the present study, these
172 observations are used only to ensure the absence of the ice phase. This 2DC-Grey was
173 also modified with new tips to reduce shattering artifacts (Korolev et al., 2011), and it
174 was mounted in a canister beside the FSSP-100.
- 175 g) Carbon monoxide (CO) is used here as a relative indicator of aerosol influenced by
176 pollution sources and as a potential tracer for aerosol particles entering cloud. The CO
177 was measured with an Aerolaser ultra-fast carbon monoxide monitor model AL 5002
178 based on VUV-fluorimetry, employing the excitation of CO at 150nm. The instrument
179 was modified such that in-situ calibrations could be conducted in flight.
- 180
- 181 Details of the instrument calibration and evaluations are given in the Supplement (S1).



182

183 **2.1 State parameters and Winds**

184

185 State parameters and meteorological measurements were measured with an AIMMS-20,
186 manufactured by Aventech Research Inc. The instrument consists of three modules: 1) an Air
187 Data Probe that measures the three-dimensional aircraft-relative flow vector (true air speed,
188 angle-of-attack, and sideslip), temperature and relative humidity, and includes a three-axis
189 accelerometer pack for turbulence measurement; 2) an Inertial Measurement Unit that consists of
190 three gyros and three accelerometers providing the aircraft angular rate and acceleration; 3) a
191 Global Positioning System for aircraft 3D position and inertial velocity. Horizontal and vertical
192 wind speeds are measured with accuracies of 0.50 and 0.75 m/s, respectively; the vertical
193 resolution was insufficient to measure gusts in the sampled clouds. The accuracy and resolution
194 for temperature measurement are 0.30 and 0.01 C. The accuracy and resolution for relative
195 humidity measurement are 2.0 and 0.1 %. The sampling frequency is 1 Hz.

196

197 **2.2 Inlets**

198

199 Aerosol particles were sampled through a shrouded inlet diffuser (diameter of 0.35 cm at intake
200 point), which is the same inlet discussed by Leaitch et al. (2010). Transmission of particles by
201 the inlet is approximately unity for particles from 20 nm to <1 μm and at the airspeeds operated
202 at here. The intake was connected inside the cabin to a 1.9 cm OD stainless steel manifold off
203 which sample lines were drawn to the various instrument racks using angled inserts. The total
204 flow at the intake point was approximately isokinetic at 55 L min^{-1} based on the sum of flows



205 drawn by the instrumentation (35 L min^{-1}) and the measured flow at the exhaust of the tube. The
206 flow at the exhaust of the tube was allowed to flow freely into the back of the cabin so that the
207 flow at the intake varied by the aircraft TAS and the manifold was not significantly over
208 pressured.

209 CO was sampled through a separate inlet consisting of a 0.40 cm OD Teflon tube using
210 the forward motion of the aircraft to push air into the line in combination with a rear-facing 0.95
211 cm OD Teflon exhaust line that lowered the line pressure. The continuously measured sample
212 flow was approximately 12 L min^{-1} .

213

214 **2.3 Approach to Analysis**

215

216 Eleven research flights were conducted from Resolute Bay, Nunavut ($74^{\circ}40'48''\text{N } 94^{\circ}52'12''\text{W}$)
217 beginning July 4 and ending July 21, 2014. The measurements were associated with two
218 relatively distinct weather regimes. During period 1 (July 4-12), the weather conditions around
219 Resolute Bay were affected by an intensive upper low (Supplement Fig. S4). The wind speeds at
220 500 hPa were mostly calm and varying from south to north. The surface (1000 hPa) was
221 dominated by weak high-pressure with generally clear skies, light winds, and occasional
222 scattered to broken stratocumulus. Low-cloud or fog was at times present in association with
223 open water, and the air was relatively clean as discussed below. There was a transition period
224 from July 13-16 when flights were not possible due to fog at Resolute Bay. During period 2 (July
225 17-21), the area came under the influence of a deep low pressure system to the south
226 (Supplement Fig. S5) that brought more wind and higher cloud. The air was not as clean as
227 during period 1, based on the measured aerosol mass and CO concentrations (see Table 1), in



228 part due to transport of BB aerosol from the Northwest Territories by the low (Köllner et al.,
229 2015). A separate analysis, based on the bulk Richardson number and data from radiosondes,
230 estimated boundary-layer heights at 254 m (± 155 m) (Aliabadi et al., 2015).

231 A summary of all flight tracks is shown in Fig. 1. Flights mostly consisted of vertical
232 profiles and of low level flying over ice, water and melt ponds that contributed to the formation
233 of low cloud, where low cloud is defined here as cloud tops below 200 m above the surface.
234 Higher level cloud was also sampled during the profiles and transits. The polynyas that were
235 sampled over are shown in the top center of each panel of Fig. 2. Cloud was sampled on eight of
236 the 11 flights, more frequently during period 1 because of better visual contrast at lower levels
237 and because period 2 marked the presence of the Canadian Coast Guard Ship Amundsen in
238 Lancaster Sound (bottom center of each panel in Fig. 2) when the flight plans were focused
239 towards sampling of the ship's plume.

240 All aerosol number concentrations are given in terms of standard atmospheric pressure
241 and temperature (STP: 1 atm and 15°C). The CDNC are also referenced to STP where
242 comparisons are made with the aerosol number concentrations. Number concentrations greater
243 than 100 nm (N100) are taken from the UHSAS. All data, except for the SMS, are 1 second
244 averages that represent a sampling path length of 60–80 m. The size distributions over 20–100
245 nm are from the SMS data, which are 1-minute averages. Except for the example shown in Fig.
246 S3, all number concentrations of particles smaller than 100 nm are taken from the SMS. N_x -100
247 refers to the number concentration within the interval “x-100” where x ranges between 20 and
248 90. Values of N_x with $x < 100$ are derived from the sum of N_x -100 (SMS) + N100 (UHSAS).

249 Clouds were sampled when they were present in the area of study, ideally by ascending
250 or descending through them. The latter was usually possible for the higher-altitude clouds but



251 seldom possible for the low-altitude clouds. Nearly all clouds sampled were liquid phase, and
252 only liquid phase clouds are discussed here based on based on the 2DC-Grey images. Droplet
253 sizes are represented by the volume-weighted mean diameter (VMD), which has the property
254 that the VMD can be used with the CDNC to calculate the LWC.

255 The pre-cloud aerosol is determined from averages of values collected within about 50 m
256 of cloud base where a cloud base was clear and achievable. In other cases the pre-cloud aerosol
257 are the values at the similar or lower altitudes in the clear air upwind of the cloud. For the
258 aerosol measurements made with the 1-minute averaged number concentrations from the SMS,
259 values from further below-cloud are necessary in some cases. These values are however
260 consistent with the 1-second aerosol measurements closer to cloud base. In sections 2.4.1 and
261 2.4.2, detailed examples are used to show how the aerosol observations relate to the cloud
262 observations for the higher-altitude (HA) cloud (clouds based above 200 m) and low-altitude
263 (LA) cloud (clouds topped below 200 m), and to demonstrate how the pre-cloud aerosol
264 concentrations were assessed.

265

266 **2.4.1 Higher Altitude (HA) Cloud Examples**

267

268 Four examples of profiles through HA clouds are shown in Fig. 3. There are two panels for each
269 profile: the left-hand panel shows CO, CDNC and particle number concentrations (N₅, N_{x-100},
270 N₁₀₀, CCNC); the right-hand panel shows temperature, equivalent potential temperature (θ_e),
271 LWC and VMD. The temperatures, θ_e and VMD are scaled as indicated.

272 July 7 Case (Fig. 3 a, b): One of several profiles through a stratocumulus layer on July 7
273 sampled during the transits to and from the polynyas north of Resolute Bay. The CDNC (at STP)



274 are relatively constant with altitude and the LWC and VMD both increase steadily with altitude,
275 features common to the formation of cloud by lifting of air and indicating that the cloud droplets
276 were nucleated on particles in air rising from cloud base. The cloud top is capped by a
277 temperature inversion of about 2°C at 2350 m, and the particle profiles along with θ_e and CO are
278 relatively constant below the cloud base. In-cloud, the number concentrations of larger particles
279 (N100) is reduced due to scavenging by the cloud droplets; although such particles are not
280 completely eliminated as smaller droplets can enter the inlet and dry in the sampling lines.
281 Smaller particles can be artificially increased in cloud due to the shattering of larger droplets on
282 the aerosol intake, as indicated by the increase in the N5 higher in the cloud. The in-cloud
283 aerosol measurements are shown here only for completeness, but they are not used in the
284 subsequent analysis. The CDNC range up to 265 cm⁻³ and the mean value is 199 cm⁻³. Below
285 cloud base, the N5, N20-100, N30-100, N50-100, N100 and CCNC are approximately 235 cm⁻³,
286 167 cm⁻³, 145 cm⁻³, 94 cm⁻³, 67 cm⁻³ and 117 cm⁻³, respectively. The below-cloud N20 of 234
287 cm⁻³ approximately equals the N5 offering confidence in terms of the closure of number
288 concentrations. The N30 values compares most closely with the mean CDNC leading to the
289 conclusion that in the mean cloud droplets nucleated on particles down to about 30 nm; see
290 Supplement Fig. S6a. It is possible that particles as small as 20 nm contributed to the CDNC in
291 this cloud based on the maximum CDNC; for 20 nm particles to activate, the water
292 supersaturations in the bases of the clouds would have had to reach about 1.5%. The below-cloud
293 number size distribution for this case is compared with a below-cloud case from over the western
294 Atlantic Ocean (S.I. Fig. S6a). The overall particle concentration is much higher in the Atlantic
295 Ocean case, and the activation size is correspondingly higher at about 110 nm. There are some
296 differences in activation due to differences in updraft speeds, but the volume concentration of



297 particles larger than 100 nm in the Atlantic case is more than 30 times higher than the present
298 case of July 7 (S.I. Fig. 6b). The much lower volume concentration of larger particles in the July
299 7 case will lower water uptake during the initial stages of growth, resulting in a higher maximum
300 supersaturation.

301 July 17 Case (Fig. 3 c, d): The July 17 profile is similar in some respects to the July 7
302 case, but there is more variability near the cloud top and the CDNC (STP) are overall lower with
303 a maximum of about 75 cm^{-3} and a mean of 55 cm^{-3} . The VMD exceed $20 \mu\text{m}$ compared with a
304 peak value of about $15 \mu\text{m}$ for the July 7 profile. Continuity from about 100 m below cloud base
305 is indicated by the CO and θ_e profiles, and the N50 approximates the mean CDNC and possibly
306 the maximum CDNC. The CCNC are $30\text{--}40 \text{ cm}^{-3}$ below cloud, indicating a supersaturation larger
307 than 0.6%.

308 July 19 Case (Fig. 3 e, f): The July 19 profile includes two cloud layers, one from 1200-
309 1400 m and the second from 1400-1500 m. The layer separation appears in the CO
310 concentrations, which are uniform through the lower layer and increasing in the upper layer. The
311 CO levels of 100+ ppbv in this case are among the highest observed during the study, reflecting
312 contributions from BB as discussed by Köllner et al. (2015). The mean CDNC (STP) in the
313 lower and upper layers are 239 cm^{-3} and 276 cm^{-3} respectively. The VMD reach $15 \mu\text{m}$ in the
314 lower layer and are smaller in the upper layer. The smaller VMD is influenced by the lower
315 LWC and the slightly higher CDNC, where the latter may be governed by the increase in aerosol
316 from below the layer to above the layer. The N50 and N100 estimated for the lower (upper)
317 layer are $269 (334) \text{ cm}^{-3}$ and $197 (221) \text{ cm}^{-3}$ respectively. Thus, in the mean the CDNC in both
318 layers are approximated by the activation of particles sized between 50 nm and 100 nm, and the
319 maximum CDNC suggests activation of particles down to about 50 nm. The CCNC are slightly



320 below the N100 possibly due to a reduced hygroscopicity of the BB particles. Comparison of the
321 CCNC with the CDNC suggests cloud supersaturations above 0.6%.

322 July 20 Case (Fig. 3 g and h): A more complex cloud with substantial variations in the
323 LWC that suggests three cloud layers. The values of the mean CDNC at STP are 45 cm^{-3} , 49 cm^{-3}
324 3 and 65 cm^{-3} in the upper, middle and lower layers respectively. The VMD reach about $20 \mu\text{m}$
325 in the lower layer and $26 \mu\text{m}$ in the upper layer with the lower CDNC. The layers are relatively
326 stable with CO and θ_e increasing slightly from below the cloud to above the top cloud layer. The
327 N50 just below the lower layer approximately equal the CDNC in that layer. It is more difficult
328 to estimate the pre-cloud aerosol for the middle and upper layers, but particles at least as small as
329 50 nm were activated. For the summary statistics, the respective pre-cloud N100, N50 and
330 CCNC are estimated at 24 cm^{-3} , 44 cm^{-3} and 24 cm^{-3} for the upper cloud layer, 32 cm^{-3} , 52 cm^{-3}
331 and 32 cm^{-3} for the middle layer and 34 cm^{-3} , and 66 cm^{-3} and 35 cm^{-3} for the lower layer.
332 Comparison of the CCNC with the CDNC suggests supersaturations near or in excess of 0.6%.

333

334 2.4.2 Low-Altitude (LA) Examples

335

336 July 5 and July 7 Cases: The two examples in Fig. 4 are for cloud or fog over the polynyas north
337 of Resolute Bay on July 5 and July 7. Four cloud samples were collected on July 5 at altitudes
338 below 200 m . The time series in Fig. 4a covers the period of collection of the two lowest
339 samples: 16:18:02-16:21:57 at 130 m and 16:39:35-16:40:18 at 88 m . In the air upwind of the
340 cloud or fog, the N100, N30 and CCNC are estimated at 3 cm^{-3} , $10\text{-}14 \text{ cm}^{-3}$ and 5 cm^{-3} . The
341 mean values of the CDNC of 2.8 cm^{-3} at 130 m and 0.7 cm^{-3} at 88 m are explained by the N100
342 and supersaturations less than 0.6%. The maximum CDNC of 12 cm^{-3} at 130 m suggests the



343 activation of smaller particles, possibly as small as 30 nm, and a supersaturation exceeding 0.6%
344 perhaps due to some uplift influenced by orographic features north of the north polynya. At 88
345 m, the mean VMD (not shown) was 29 μm and ranged up to 35 μm giving those droplets
346 potential to deposit over an hour or more, thereby transferring water from the polynya to the
347 downwind ice. On July 7, cloud or fog was present below 120 m and thicker towards the north
348 edge of the north polynya and again to the north over the ice. The CDNC are overall higher with
349 averages of seven samples over the period 16:06-16:29 ranging from 4 cm^{-3} to 13 cm^{-3} , the one-
350 second CDNC are as high as 34 cm^{-3} and the mean VMD (not shown) range from 19.6 μm to
351 22.8 μm . The CO mixing ratio is slightly higher in the cloud (81 ppbv) than above (79 ppbv). In
352 the air nearly free of cloud and below 120 m, the N100 are 4-5 cm^{-3} , the N50 are 8-11 cm^{-3} and
353 the N20 are variable between 17 cm^{-3} and 130 cm^{-3} ; CCN are unavailable for this part of the
354 flight due to instrument problems. Mean values of CDNC/N100 and CDNC/N50 for seven cloud
355 samples are 4.8 and 1.0, respectively, indicating that on average particles about 50 nm were
356 activated in this LA cloud. Based on the overall relationship between CCNC and N50, which is
357 discussed in section 3.3, the mean supersaturation in the LA cloud of July 7 is estimated at 0.6%.
358 Comparison with the maximum CDNC suggests that particles as small as 20 nm may have
359 participated in the nucleation of droplets.

360 July 8 Case: Fig. 5 shows a time series of altitude, CO, N100, N80-100, N90-100, CCNC
361 and CDNC from the sampling above and in the low cloud over Lancaster Sound on July 8. The
362 cloud over the open water of the Sound is visible in the satellite picture in Fig. 2b. Cloud was
363 also present over the ice to the west, but it was much thinner and reached only to about 150 m.
364 Over the water, the cloud was sampled as high as 230 m by descending into it down to about 150
365 m between 17:27 UT and 17:43 UT as shown in Fig. 5. Observations in profiles from two of the



366 five samples are shown in Fig. 6. The cloud deepened as the aircraft approached the ice edge
367 from over the water, and thinned abruptly over the ice with tops below 150 m as shown in Fig. 5
368 (time 17:47). The thicker cloud was associated with a shift in the wind direction to be more
369 southerly suggesting an influence of the Prince Regent Inlet and surrounding terrain on the flow
370 as well as possibly circulations influenced by the water-ice transition. The cloud layer was
371 relatively stable and the θ_e profiles suggest a surface heat sink (Fig. 6a). The profiles of LWC
372 and VMD in Fig. 6 (b, c) do not show increases with altitude characteristic of vertical mixing,
373 such as for some of the HA clouds (Fig. 3); the change in the VMD per 50 m increase in height is
374 about $1.7 \mu\text{m}$ for the well mixed cloud of July 7 (Fig. 3 a, b), whereas it is about $0.2 \mu\text{m}$ per 50 m
375 for the LA cloud of flight 8 in Fig. 6. The CO mixing ratio shows little variation with time and
376 altitude. The pre-cloud aerosol concentrations are more difficult to assess. Based on
377 concentrations just above the cloud, particles $>90 \text{ nm}$ explain the CDNC. Based on the
378 concentrations downwind at 150 m (approximately 17:47), activation of particles $>80 \text{ nm}$ is
379 needed to explain the CDNC. The CCNC are about 129 cm^{-3} downwind and between 157 cm^{-3}
380 and 234 cm^{-3} just above cloud. It is concluded that in this case the droplets likely nucleated on
381 particles mostly larger than 80-95 nm and the supersaturations in the clouds were less than 0.6%.
382 For the purposes of summary statistics discussed next, the N100, N50 and CCNC have been
383 selected as an average of the downwind and immediately above cloud concentrations: 73 cm^{-3} ,
384 319 cm^{-3} and 168 cm^{-3} , respectively.
385
386



387 **3. Summary Observations and Discussion**

388

389 Summary statistics for the cloud and aerosol samples are discussed in 3.1, the microphysics of
390 low-altitude and higher-altitude clouds are contrasted in 3.2, particle activation is summarized in
391 3.3 and in section 3.4 the relationship between VMD and CDNC is used to consider the
392 transition of aerosol indirect effects from potential warming to potential cooling.

393

394 **3.1 Summary of mean observations**

395

396 A total of 62 liquid water cloud samples were averaged where the mean LWC was $> 0.01 \text{ g m}^{-3}$.
397 The samples are integrations over periods ranging from 11 seconds to 1000 seconds with a
398 median sample time of 65 seconds that is equivalent to a horizontal path length of about four
399 kilometers. The mean and median values of the microphysical properties of the aerosols and
400 clouds as well as the altitudes and temperatures associated with the 62 cloud samples are given in
401 Table 1, separated between periods 1 and 2. Values of the CDNC and the LWC are given relative
402 to in-situ volumes as well as STP. As discussed above, the pre-cloud CCNC, N50, and N100 are
403 averages of those values collected within about 50 m of cloud base where a cloud base was clear
404 and achievable. In other cases the pre-cloud CCNC, N50 and N100 are the values at the similar
405 or lower altitudes in the clear air upwind of the cloud, except in the case of July 8 when the pre-
406 cloud aerosol is based on the measurements in the area downwind plus those immediately above
407 cloud. The CCNC samples in Table 1 are limited to 44 due to instrument problems, all of which
408 occurred during the early part of July 7.



409 Cloud liquid water paths (LWP) are estimated for 36 of the samples when a complete
410 profile between cloud base and cloud top was possible. The LWP are shown at the bottom of
411 Table 1. Thirty-four of the 36 LWP estimates are for above 200 m, and the mean and median
412 altitudes are 1044 m and 862 m, respectively. Not included in the summary statistics are the
413 samples from July 8 shown in Figs 5 and 6. For the minimum altitude reached in that cloud, the
414 LWP ranged from 12 to 25 and thus the total LWP for that cloud ranged to above 25.

415 During period 1, the median sampling altitude is lower and the temperatures are slightly
416 below freezing compared with just above freezing during period 2. The CO mixing ratios are
417 overall low and at approximately background values during period 1. The median CDNC are
418 higher during period 1 than period 2, but the mean values are similar. The CDNC compare more
419 closely with the N50 during period 1, while during period 2 the CDNC are about equally
420 between the N50 and N100. The CCNC equated with particles between 50 nm and 100 nm
421 during period 1, whereas during period 2 they were closer to the N100 values. The reduction in
422 particle hygroscopicity during period 2 may be due to an increased presence of organics in the
423 aerosol during that time (Willis et al., personal communication).

424

425 **3.2 Comparison of LA and HA cloud**

426

427 The LA clouds are associated with low-level horizontal advection and heat and water exchange
428 with the underlying ice or water surface. In contrast, vertical motions are responsible for some of
429 the HA clouds, and none of the HA clouds interact so closely with the underlying surface. Due to
430 those differences, the characteristics of the LA and HA clouds are considered separately. Table 2
431 shows the mean and median values for the samples separated between LA and HA clouds;



432 vertical profiles of the CDNC, LWC and VMD samples are shown in Supplement Fig. S7. On
433 average, the LA samples have lower CDNC and higher VMD compared with the HA cases, and
434 the LA clouds are activating on larger particles relative to the HA clouds (e.g. CDNC/N50). The
435 values of the CDNC/CCNC indicate that the supersaturations are <0.6% for the LA clouds and
436 close to 0.6% for the HA clouds.

437 Variations in LWC are correlated with those of CDNC for the LA samples (Fig. 7a). The
438 coefficient of determination (R^2) rises from 0.57 to 0.98 if the one LA point at (137, 0.032) is
439 removed. In contrast, the correlation of the LWC with the CDNC for the HA samples is low
440 ($R^2=0.16$). There is no correlation of the LWC with the VMD for the LA points ($R^2=0.04$), and
441 for the HA clouds there is a modest correlation of LWC with MVD ($R^2=0.26$). Variations in
442 LWC with VMD within a cloud system are consistent with lifting of air from below, i.e.
443 nucleation of droplets at cloud base followed by their growth with increasing altitude, such as the
444 case shown in Fig. 3a and 3b. They can also result from homogeneous mixing (i.e. entrainment
445 of dry air that reduces the LWC by evaporation of the droplets without reducing the CDNC). The
446 strong dependence of the variations in LWC with those of the CDNC in the LA clouds may
447 reflect changes in rate of cooling, collision-coalescence or inhomogeneous mixing along the
448 cloud transport pathway. For example, increases in the rate of cooling within or between clouds
449 will increase condensation rates, and potentially supersaturations, resulting in increased LWC
450 and CDNC. Reductions in the collision-coalescence process will result in higher CDNC and
451 lower deposition rates that can increase the LWC. Inhomogeneous mixing, the entrainment of
452 dry air parcels into a cloud without mixing with the cloud droplets, will reduce the CDNC
453 averaged across the cloud and at the same time reduce the mean LWC. Changes in the aerosol,



454 which are interactive with some of the cloud processes, may contribute to the CDNC and
455 potentially the LWC through their influence on collision-coalescence.

456 The LWC-CDNC correlation is identifiable for individual flights with sufficient LA
457 samples: four flights, comprising 20 of the 24 LA samples, had three or more points as shown in
458 Fig. 8. The regressions for each of the July 7, 8 and 17 cases are approximately linear, and the
459 respective mean VMD are 20.8 μm , 18.8 μm and 18.2 μm . The mean LWC are 0.05 g m^{-3} , 0.3 g
460 m^{-3} and 0.07 g m^{-3} . The VMD are relatively close together confirming similarities in the
461 relationship, even if it not purely linear. For comparison, the mean VMD for the July 5 samples
462 is 29.2 μm and the LWC is 0.02 g m^{-3} , which indicates that the July 5 case does not fit the linear
463 relationship shown in Fig. 8a. The reasons behind the similarity of the VMD for the July 7, 8 and
464 17 are unknown, but it occurs despite the varied pre-cloud N50 and N100: N50 range of 5-272
465 cm^{-3} ; N100 range of 1.1-73 cm^{-3} . The consistencies among the three flights for greatly differing
466 aerosol and CDNC imply a much smaller role for the aerosol in terms of the LWC. The
467 distributions of droplets extend above 20 μm in these cases, but few are of sufficient size to
468 initiate collision-coalescence (about 30 μm) (e.g. Rosenfeld et al., 2001) unless some fall out
469 already had occurred. Greater temporal and spatial coverage are needed to assess the
470 microphysical processes in these clouds.

471

472 3.3 Particle Activation Sizes

473

474 Here, the sizes and CCN activity of particles that acted as nuclei for cloud droplets are examined.
475 As shown in the plot of CDNC versus N100 (Fig. 9a), particles smaller than 100 nm activated in
476 most cases and most often in the HA clouds. The mean and median values of CDNC(STP)/N100



477 are 2.2 and 1.8 for all 62 samples, and the 30th percentile of the CDNC/N100 is 1.2, which means
478 that in about 70 % of the cases droplets nucleated on particles significantly smaller than 100 nm.
479 Fig. 9a can be compared with the results of Hegg et al. (2012) who showed a linear fit of CDNC
480 to N100 for marine stratocumulus with a slope of 0.72 for which the N100 in 94% of the samples
481 was $>150 \text{ cm}^{-3}$. Here, a slope larger than unity is indicated, and the N100 are $<100 \text{ cm}^{-3}$ in 90%
482 of the samples. The comparison indicates that relationships derived for higher concentration
483 environments do not necessarily apply to those to lower concentration environments. In the clean
484 environment often found in the Arctic during summer, the absence of larger particles may lower
485 water uptake rates during droplet nucleation, which will increase the supersaturation, enabling
486 cloud droplets to nucleate on smaller particles; the absence of larger particles may also help
487 increase the concentrations of smaller particles in the Arctic during summer, by promoting new
488 particle formation through a reduced condensation sink (e.g. Leaitch et al., 2013). The CDNC are
489 plotted against the N50 in Fig. 9b showing that the mean activation size was often close to 50
490 nm. The median value of CDNC/N50 is 0.78 for all samples indicating that, based on the
491 averaged CDNC, cloud droplets nucleated on particles near or smaller than 50 nm about 40% of
492 the time. That percentage will increase if particle activation is considered relative to the
493 maximum CDNC.

494 The mean and median values of the CCNC associated with all cloud samples (84 cm^{-3}
495 and 47 cm^{-3}) are generally consistent with previous Arctic CCNC measurements. For example,
496 during the summer above 85°N , Martin et al. (2011) measured a mean CCNC at 0.73%
497 supersaturation of 47 cm^{-3} with a standard deviation of 35 cm^{-3} , and Yum and Hudson (2001)
498 measured CCNC at 0.8% supersaturation below 1700 m over the Beaufort Sea during May, 1998
499 that ranged from 41 cm^{-3} to 290 cm^{-3} . Considering the median values of CDNC/CCNC for the



500 LA and HA samples (Table 2) and the slopes of linear regressions of CDNC versus CCNC (Fig.
501 10a), the average inferred supersaturation for the HA clouds is about 0.6%, consistent with the
502 overall activation of smaller particles in those clouds. The mean supersaturation inferred for the
503 LA clouds is significantly lower than 0.6%. Based on the activation of a 90 nm particle (July 8
504 case; CCNC of 168 cm^{-3} in Fig. 10a) of low-moderate hygroscopicity, a reasonable estimate is
505 0.3% for the mean of the LA clouds with some higher values indicated by the points near a
506 CCNC of 25 cm^{-3} in Fig. 10a. The supersaturations for these clean clouds are in contrast to
507 polluted marine environments for which estimates for these types of clouds are 0.2% or less (e.g.
508 Modini et al., 2015). Consistent with the present results, Hudson et al. (2010) found that effective
509 supersaturations in marine stratus tended to increase with a decrease in the CCNC, and for
510 CCNC smaller than about 200 cm^{-3} their effective supersaturations ranged between 0.3% and
511 1.2%.

512 Variations in the measured CCNC are explained well by variations in smaller (N50) and
513 larger (N100) particles as shown in Fig. 10b. The slopes of the power-law fits, for which the
514 exponents are both close to unity, indicate that the CCNC at 0.6% supersaturation on average fall
515 between 50 nm and 100nm.

516

517 **3.4 Aerosol Influences on Warming to Cooling**

518

519 Here, the aerosol influence on clouds with CDNC below the Mauritsen-limit and the potential
520 background influence of the aerosol on clouds with CDNC above the Mauritsen-limit are
521 considered. The relationship between the VMD and CDNC, shown in Fig. 11, exhibits a
522 scattered but clear tendency for smaller VMD with increasing CDNC. The solid black curve is a



523 reference line based on the study-mean LWC of 0.12 g m^{-3} (Table 1); points falling above or
524 below the black curve have higher or lower LWC, respectively. The vertical dashed green line
525 represents the Mauritsen limit below which the cloud may produce a net warming for an increase
526 in the CDNC. The net warming is a consequence of an increase in longwave absorption due to an
527 increase in the LWC, where the latter results from a reduction in deposition for the smaller
528 droplets associated with increased CDNC. Above the Mauritsen limit, an increase in CDNC may
529 produce a net cooling due to the cloud albedo effect, since at that point the longwave forcing
530 does not change significantly as the effects of deposition are minimized and the cloud effectively
531 behaves as a black body.

532

533 3.4.1 Below the Mauritsen limit

534

535 Seventeen of the 62 samples fall at or below the Mauritsen limit, which is suggested here as 16
536 cm^{-3} . The value of 16 cm^{-3} is selected because all points fall below the mean LWC, and these
537 points offer greater potential for changes in the CDNC to increase the LWC. Fifteen of the 17
538 samples are from LA clouds with median pre-cloud N50 and N100 estimates of 8.2 cm^{-3} and 3.0
539 cm^{-3} respectively. The lower number concentrations contribute to overall larger VMD; although
540 some of the points below the Mauritsen limit have VMD values much less than $20 \mu\text{m}$. Increases
541 in small particles, potentially from particle nucleation or fragmentation (e.g. Leck and Bigg,
542 1999 and 2010), are hypothesized to increase the CDNC thereby enhancing the longwave
543 warming by these clouds at least until the CDNC reach above the Mauritsen limit. The LA points
544 from the July 5 and the July 7 cases, identified in Fig. 11, offer one insight. Considering the
545 median CDNC for July 5 is eight times lower than that for July 7, the absence of a similar



546 difference in the N50 and N100 for July 5 and July 7 (see Fig. 11 caption) suggests the aerosol
547 was not a factor in the differences in CDNC. Consistent with the discussion in section 3.2, all 15
548 LA points show a correlation of LWC with the CDNC ($R^2=0.57$), but correlations of the CDNC
549 with the N50 and N100 are weak: $R^2=0.19$ and 0.06 , respectively. Because only seven points
550 with CCNC are available, which correlate well with the N50, the CCN are not used here. If the
551 Mauritsen limit of 10 cm^{-3} is applied, reducing the number of points to 12, the assessment does
552 not change: the LWC-CDNC correlation improves slightly and the correlations of the CDNC
553 with the N100 and the N50 weaken. Also, the LWC do not correlate with either the N50 or the
554 N100 (Supplement Fig. 8). In this low CDNC environment, where cloud droplets may grow
555 large enough to be gravitationally removed from the cloud without the support of collision-
556 coalescence, the absence of a positive correlation of either the CDNC or LWC with the aerosol
557 indicates that changes in the aerosol did not contribute significantly to the changes in the LWC.
558 Variations in other processes, such as mixing or the rate of cooling, may be responsible for the
559 correlation of CDNC and LWC. In these cases, there is sufficient aerosol so as not to be a
560 limiting factor for the CDNC.

561

562 3.4.2 Background aerosol influence on clouds

563

564 Above the Mauritsen limit, the general reduction in the VMD with the CCNC-associated
565 increase in CDNC reflects the aerosol impact on the clouds. In Fig. 11, samples are identified
566 between those associated with lower CO (green circles; <81 ppbv, the median CO value of all
567 samples) and those with highest CO (red circles; >90 ppbv); six samples have no CO
568 measurement and the remaining points have CO falling within 81-90 ppbv. Five of the seven



569 higher-CO samples are from the July 19 case (e.g. Fig. 3e, 3f) that has been linked with BB
570 (Köllner et al., 2015; reference above), and the highest CDNC point (273 cm^{-3} ; no CO
571 measurement) is also from July 19 and likely influenced by BB. The higher-CO samples cover a
572 range of CDNC from 16 cm^{-3} to at least 238 cm^{-3} with CO reaching up to 113 ppbv. The higher
573 CO samples are associated with larger particles ($N_{50}/N_{100}=1.5$), consistent with a BB influence,
574 compared with the lower CO samples ($N_{50}/N_{100}=3.2$). These values for BB fall at the low end
575 of the observations from Zamora et al. (2015), but their CO concentrations are much higher than
576 those measured in this study. The lower-CO samples may be dominated by regional biogenic
577 emissions (Burkart et al., 2015). The lower- and higher-CO points overlap over a CDNC range
578 of 16 cm^{-3} to 160 cm^{-3} , consistent with the range of pre-industrial CDNC from global models of
579 30 cm^{-3} to 140 cm^{-3} (Penner et al., 2006) and suggesting that 20-100 nm particles from natural
580 sources can have a broad impact on the range of CDNC in clean environments. This result
581 affirms the large uncertainty associated with estimating a baseline for the cloud albedo effect
582 discussed by Carslaw et al. (2013).

583

584 **4. Summary and Conclusions**

585

586 Aerosol particle size distributions, CCNC at 0.6% water supersaturation, carbon monoxide (CO)
587 and cloud microphysics were measured from an airborne platform based out of Resolute Bay,
588 Nunavut from July 4 to July, 21, 2014 as one part of the Canadian NETCARE project. The
589 flights were conducted over ice and water surfaces from about 60 m above the surface to about
590 6000 m. Sixty-two (62) cloud-averaged samples were derived, each constrained for the mean
591 $\text{LWC} > 0.01 \text{ g m}^{-3}$. The analysis separates the cloud samples between 24 low-altitude (LA: < 200



592 m) samples and 38 higher altitude (HA: >200 m) samples as well as situations of lower and
593 higher CO and observations above and below the Mauritsen et al., (2011) CCNC (or CDNC)
594 limit.

595 The median pre-cloud N100 of 33 cm^{-3} and the median CO mixing ratio of 81 ppbv
596 indicate that the aerosols supporting the sampled clouds were relatively clean, and particularly
597 during the first part of the study many of the aerosol particles may have been derived from
598 regional natural sources. The median CDNC at STP is 10 cm^{-3} for the LA clouds (24 samples)
599 and 101 cm^{-3} for the HA clouds (38 samples), which correspond with the median pre-cloud N50
600 of 11 cm^{-3} for the LA samples and 133 cm^{-3} for the HA samples. The lower sizes of particles
601 activated in cloud varied from about 20 nm to above 100 nm. In 40% of cases, the average lower
602 size of activation was 50 nm or smaller. Overall, smaller particles were activated more often in
603 the HA clouds.

604 From the median values of CDNC/CCNC (1.2 for the HA clouds and 0.6 for the LA
605 clouds) and linear regression of CDNC and CCNC, it is inferred that the average
606 supersaturations were approximately 0.6% for the HA clouds and 0.3% for the LA clouds.
607 Higher estimates will be obtained if the maximum CDNC are taken into consideration rather than
608 the mean CDNC. The relatively high supersaturations for these clean Arctic stratus and
609 stratocumulus have similarities with the observations of Hudson et al. (2010) for stratus off the
610 coast of California.

611 In 17 cases, 15 of which are LA clouds, the CDNC fell at or below the CCN limit
612 discussed by Mauritsen et al. (2011), which is estimated here as 16 cm^{-3} . These are the first
613 collection of simultaneous observations of the microphysics of aerosols and clouds in this unique
614 regime in which the net radiative impact of increases in the CDNC is hypothesized to be



615 warming due to changes in the LWC. The LWC of the points below the Mauritsen limit all fall
616 below the study-mean LWC, and the LWC increases with the CDNC. Neither the CDNC nor the
617 LWC are positively correlated with the pre-cloud aerosol (N50 or N100). In this environment of
618 low cloud or fog and ultra-low CDNC, variations in cloud processes such as mixing or the rate of
619 cooling may be responsible for the correlation of CDNC and LWC, whereas the aerosol is
620 generally sufficient so as not to be the factor limiting the CDNC or LWC.

621 Forty-five cloud samples with CDNC above the Mauritsen limit exhibit a clear influence
622 of the aerosol. The cloud microphysics for the clouds formed in cleaner air (smaller particles and
623 lower CO: <81 ppbv) overlap with clouds formed in more polluted air (larger particles and
624 higher CO: >90 ppbv) covering a CDNC range of 16-160 cm⁻³. It is concluded that 20-100 nm
625 particles from natural sources can have a broad impact on the range of CDNC in clean
626 environments, affirming a large uncertainty in estimating a baseline for the cloud albedo effect.

627

628



629 *Acknowledgements.* The complete data set is available from the NETCARE web site by
630 contacting Richard Leaitch (Richard.Leaitch@ec.gc.ca) or Jon Abbatt
631 (jabbatt@chem.utoronto.ca). A spreadsheet containing the details of the 62 samples discussed
632 here is included with the supplement. The authors acknowledge a large number of people for
633 their contributions to this work. We thank Kenn Borek Air, in particular Kevin Elke and John
634 Bayes for their skillful piloting that facilitated these cloud observations. We are grateful to John
635 Ford, David Heath and the U of Toronto machine shop, Jim Hodgson and Lake Central Air
636 Services in Muskoka, Jim Watson (Scale Modelbuilders, Inc.), Julia Binder and Martin
637 Gerhmann (AWI), Mike Harwood and Andrew Elford (EC), for their support of the integration
638 of the instrumentation and aircraft. We thank Mohammed Wasey for his support of the
639 instrumentation during the integration and in the field. We are grateful to Carrie Taylor (EC),
640 Bob Christensen (U of T), Kevin Riehl (Kenn Borek Air), Lukas Kandora, Manuel Sellmann and
641 Jens Herrmann (AWI), Desiree Toom, Sangeeta Sharma, Dan Veber, Andrew Platt, Anne Marie
642 Macdonald, Ralf Staebler and Maurice Watt (EC), Kathy Law and Jennie Thomas (LATMOS)
643 for their support of the study. We thank the Biogeochemistry department of MPIC for providing
644 the CO instrument and Dieter Scharffe for his support during the preparation phase of the
645 campaign. We thank the Nunavut Research Institute and the Nunavut Impact Review Board for
646 licensing the study. Logistical support in Resolute Bay was provided by the Polar Continental
647 Shelf Project (PCSP) of Natural Resources Canada under PCSP Field Project #218-14, and we
648 are particularly grateful to Tim McCagherty and Jodi MacGregor of the PCSP. Funding for this
649 work was provided by the Natural Sciences and Engineering Research Council of Canada
650 through the NETCARE project of the Climate Change and Atmospheric Research Program, the
651 Alfred Wegener Institute and Environment Canada.



652 **References**

653

654 Aliabadi, A. A., Staebler, R. M., de Grandpré, J., Zadra, A., and Vaillancourt, P. A.: Comparison
655 of Estimated Atmospheric Boundary Layer Mixing Height in the Arctic and Southern Great
656 Plains under Statically Stable Conditions: Experimental and Numerical Aspects, *Atmos-Ocean.*,
657 In Press, doi:10.1080/07055900.2015.1119100, 2015.

658

659 Barrie, L.A.: Arctic air pollution: An overview of current knowledge, *Atmos. Environ.*, 20, 643–
660 663, doi:10.1016/0004-6981(86)90180-0, 1986.

661

662 Barrie, L.A., Bottenheim, J.W., Schnell, R.C., Crutzen, P.J., and Rasmussen, R.A.: Ozone
663 depletion and photochemical reactions at polar sunrise in the lower Arctic atmosphere, *Nature*,
664 334, 138-141, 1998.

665

666 Brenner, T.C., Curry, J.A., and Pinto, J.O.: Radiative transfer in the summertime Arctic, *J.*
667 *Geophys. Res.*, 106, 15173-15183, 2001.

668

669 Brock, C.A., Cozic, J., Bahreini, R., Froyd, K.D., Middlebrook, A.M., McComiskey, A.,
670 Brioude, J., Cooper, O.R., Stohl, A., Aikin, K.C., de Gouw, J.A., Fahey, D.W., Ferrare, R.A.,
671 Gao, R.-S., Gore, W., Holloway, J.S., Hubler, G., Jefferson, A., Lack, D.A., Lance, S., Moore,
672 R.H., Murphy, D.M., Nenes, A., Novelli, P.C., Nowak, J.B., Ogren, J.A., Peischl, J., Pierce,
673 R.B., Pilewskie, P., Quinn, P.K., Ryerson, T.B., Schmidt, K.S., Schwarz, J.P., Sodemann, H.,
674 Spackman, J.R., Stark, H., Thomson, D.S., Thornberry, T., Veres, P., Watts, L.A., Warneke, C.,
675 and Wollny, A.G.: Characteristics, sources, and transport of aerosols measured in spring 2008
676 during the aerosol, radiation, and cloud processes affecting Arctic climate (ARCPAC) project,
677 *Atmos. Chem. Phys.*, 11, 2423–2453, 2011, doi:10.5194/acp-11-2423-2011, 2011.

678

679 Browse, J., Carslaw, K.S., Mann, G.W., Birch, C.E., Arnold, S.R., and Leck, C.: The complex
680 response of Arctic aerosol to sea-ice retreat, *Atmos. Chem. Phys.*, 14, 7543-7557,
681 doi:10.5194/acp-14-7543-2014, 2014.

682

683 Burkart, J., Willis, M., Köllner, F., Schneider, J., Bozem, H., Hoor, P.,
684 Ghahremaninezhadgharelar, R., Wentworth, G., Norman, A.L., Brauner, R., Konrad, C., Herber,
685 A., Leitch, R., and Abbatt, J.P.D.: Evidence for New Particle Formation in the Summertime
686 Arctic near Resolute Bay, Nunavut, Canada, presented at the 7th Symposium on Aerosol–Cloud–
687 Climate Interactions, American Meteorological Society, Phoenix, Arizona, 2015.

688

689 Cai, Y., Montague, D.C., Mooiweer-Bryan, W., Deshler, T.: Performance characteristics of the
690 ultra-high sensitivity aerosol spectrometer for particles between 55 and 800 nm: Laboratory and
691 field studies, *J. Aerosol Sci.*, 39, 759 – 769, 2008.

692

693 Carslaw, K.S., Lee, L.A., Reddington, C.L., Pringle, K.J., Rap, A., Forster, P.M., Mann, G.W.,
694 Spracklen, D.V., Woodhouse, M.T., Regayre, L.A., and Pierce, J.R.: Large contribution of
695 natural aerosols to uncertainty in indirect forcing. *Nature*, 503, doi:10.1038/nature12674, 2013.

696



- 697 Christensen, J. H. et al.: Chapter 14, in *Climate Change 2013, The Physical Science Basis*
698 (editors Stocker, T. F. et al.), Intergovernmental Panel on Climate Change, Cambridge Univ.
699 Press, Cambridge, U.K, 2013.
700
- 701 Curry, J.A.: Introduction to special section: FIRE Arctic clouds experiment, *J. Geophys. Res.*,
702 106, 14,985-14,987, 2001.
703
- 704 Earle, M. E., Liu, P.S.K., Strapp, J.W., Zelenyuk, A., Imre, D., McFarquhar, D.M., Shantz, N.C.,
705 and Leaitch, W.R.: Factors influencing the microphysics and radiative properties of liquid-
706 dominated Arctic clouds: Insight from observations of aerosol and clouds during ISDAC (2008),
707 *J. Geophys. Res.*, 116, D00T09, doi:10.1029/2011JD015887, 2011.
708
- 709 Engvall, A-C, Krejci, R., Strom, J., Treffeisen, R., Scheele, R.: Changes in aerosol properties
710 during spring-summer period in the Arctic troposphere, *Atmos. Chem. Phys.*, 8, 445–462,
711 doi:10.5194/acp-8-445-2008, 2008.
712
- 713 Garrett, T. J., Zhao, C., Dong, X., Mace, G.G., Hobbs, P.V.: Effects of varying aerosol regimes
714 on low-level Arctic stratus, *Geophys. Res. Lett.*, 31, L17105, doi:10.1029/2004GL019928, 2004.
715
- 716 Garrett, T. J., Maestas, M.M., Krueger, S.K., and Schmidt C.T.: Acceleration by aerosol of a
717 radiative-thermodynamic cloud feedback influencing Arctic surface warming, *Geophys. Res.*
718 *Lett.*, 36, L19804, doi:10.1029/2009GL040195, 2009.
719
- 720 Heintzenberg, J., Leck, C., and Tunved, P.: Potential source regions and processes of aerosol in
721 the summer Arctic, *Atmos. Chem. Phys.*, 15, 6487–6502, doi:10.5194/acp-15-6487-2015, 2015.
722
- 723 Hegg, D.A., Covert, D.S. Jonsson, H.H., and Woods, R.K.: A simple relationship between cloud
724 drop number concentration and precursor aerosol concentration for the regions of earth's large
725 marine stratocumulus decks, *Atmos. Chem. Phys.*, 12, 1229–1238, doi:10.5194/acp-12-1229-
726 2012, 2012.
727
- 728 Herman, G.F.: Solar radiation in summertime Arctic stratus clouds. *J. Atmos. Sci.*, 34, 1423-
729 1432, 1977.
730
- 731 Hobbs, P.V. and Rango, A.L.: Microstructures of low and middle-level clouds over the Beaufort
732 Sea, *Q. J. R. Meteorol. Soc.*, 124, 2035-2071, 1998.
733
- 734 Hudson, J.G., Noble, S., and Jha, V.: Stratus cloud supersaturations, *Geophys. Res. Lett.*, 37,
735 L21813, doi:10.1029/2010GL045197, 2010.
736
- 737 Intrieri, J. M., Shupe, M.D., Uttal, T., and McCarty, B.J.: An annual cycle of Arctic cloud
738 characteristics observed by radar and lidar at SHEBA, *J. Geophys. Res.*, 107, C10, 8030, doi.
739 10.1029/2000JC000423, 2002.
740
741



- 742 Jacob, D.J., Crawford, J. H., Maring, H., Clarke, A.D., Dibb, J.E., Emmons, L.K., Ferrare, R.A.,
743 Hostetler, C.A., Russell, P.B., Singh, H.B., Thompson, A.M., Shaw, G.E., McCauley, E.,
744 Pederson, J.R., and Fisher J.A.: The Arctic research of the composition of the troposphere from
745 aircraft and satellites (ARCTAS) mission: Design, execution, and first results, *Atmos. Chem.*
746 *Phys.*, 10, 5191–5212, doi:10.5194/acp-10-5191-2010, 2010.
- 747
748 Jouan, C., Pelon, J., Girard, E., Ancellet, G., Blanchet, J.P., and Delanoë, J.: On the relationship
749 between Arctic ice clouds and polluted air masses over the North Slope of Alaska in April 2008,
750 *Atmos. Chem. Phys.*, 14, 1205–1224, doi:10.5194/acp-14-1205-2014, 2014.
- 751
752 Klingebiel, M., de Lozar, A., Molleker, S., Weigel, R., Roth, A., Schmidt, L., Meyer, J., Ehrlich,
753 A., Neuber, R., Wendisch, M., and Borrmann, S.: Arctic low-level boundary layer clouds: In situ
754 measurements and simulations of mono- and bimodal supercooled droplet size distributions at
755 the top layer of liquid phase clouds, *Atmos. Chem. Phys.*, 15, 617–631, doi:10.5194/acp-15-617-
756 2015, 2015.
- 757
758 Köllner, F., Schneider, J., Bozem, H., Hoor, P., Willis, M., Burkart, J., Leaitch, W.R., Abbatt, J.,
759 Herber, A., Borrmann, S.: Pollution in the summertime Canadian High Arctic observed during
760 NETCARE 2014: Investigation of origin and composition, in *Geophysical Research Abstracts*,
761 17, EGU2015-5951, European Geophysical Union General Assembly 2015, Vienna, Austria,
762 2015.
- 763
764 Korolev, A.V., Emery, E.F., Strapp, J.W., Cober, S.G., Isaac, G.A., Wasey, M., and Marcotte,
765 D.: Small ice particles in tropospheric clouds: fact or artifact? Airborne icing instrumentation
766 evaluation experiment, *B. Am. Meteorol. Soc.*, 92, 967–973, 2011.
- 767
768 Lance, S., Shupe, M.D., Feingold, G., Brock, C.A., Cozic, J., Holloway, J.S., Moore, R.H.,
769 Nenes, A., Schwarz, J.P., Spackman, J.R., Froyd, K.D., Murphy, D.M., Brioude, J., Cooper,
770 O.R., Stohl, A., and Burkhart J.F.: Cloud condensation nuclei as a modulator of ice processes in
771 Arctic mixed-phase clouds, *Atmos. Chem. Phys.*, 11, 8003–8015, doi:10.5194/acp-11-8003-
772 2011, 2011.
- 773
774 Law, K.S., and Stohl, A.: Arctic air pollution: origins and impacts, *Science*, 315, 1537–1540,
775 2007.
- 776
777 Leaitch W. R., Lohmann, U., Russell, L.M., Garrett, T., Shantz, N.C., Toom-Saunty, D., Strapp,
778 J.W., Hayden, K.L., Marshall, J., Wolde, M., Worsnop, D.R., Jayne, J.T.: Cloud albedo increase
779 from carbonaceous aerosol, *Atmos. Chem. Phys.*, 10, 7669-7684, doi:10.5194/acp-10-7669-
780 2010, 2010.
- 781
782 Leaitch, W.R., Sharma, S., Huang, L., Macdonald, A.M., Toom-Saunty, D., Chivulescu, A., von
783 Salzen, K., Pierce, J.R., Shantz, N.C., Bertram, A., Schroder, J., Norman, A.-L., and Chang
784 R.Y.-W.: Dimethyl sulphide control of the clean summertime Arctic aerosol and cloud,
785 *Elementa: Science of the Anthropocene*, 1, 000017, doi: 10.12952/journal.elementa.000017,
786 2013.
- 787



- 788 Leck C., and Bigg, E.K.: Aerosol production over remote marine areas - A new route, *Geophys.*
789 *Res. Lett.*, 26, 3577-3580, 1999.
790
- 791 Leck C., and Bigg, E. K.: New particle formation of marine biological origin, *Aerosol Sci.*
792 *Technol.*, 44, 570–577, doi:10.1080/02786826.2010.481222, 2010.
793
- 794 Lohmann, U., Humble, J., Leaitch, R., Isaac, G., and Gultepe, I.: Simulations of ice clouds
795 during FIRE.ACE using the CCCMA single column model, *J. Geophys. Res.*, 106, 15123-15138,
796 2001.
797
- 798 Lubin, D. and Vogelmann, A.M.: Observational quantification of a total aerosol indirect
799 effect in the Arctic, *Tellus*, 62B, 181–189, DOI: 10.1111/j.1600-0889.2010.00460.x, 2010.
800
- 801 Martin, M., Chang, R.Y.-W., Sierau, B., Sjogren, S., Swietlicki, E., Abbatt, J.P.D., Leck, C., and
802 Lohmann, U.: Cloud condensation nuclei closure study on summer arctic aerosol, *Atmos. Chem.*
803 *Phys.*, 11, 11335–11350, doi:10.5194/acp-11-11335-2011, 2011.
804
- 805 Maslanik, J., Stroeve, J., Fowler, C., and Emery, W.: Distribution and trends in Arctic sea ice age
806 through spring 2011, *Geophys. Res. Lett.*, 38, L13502, doi:10.1029/2011gl047735, 2011, 2011.
807
- 808 Mauritsen, T., Sedlar, J., Tjernström, M., Leck, C., Martin, M., Shupe, M., Sjogren, S., Sierau,
809 B., Persson, P.O.G., Brooks, I.M., and Swietlicki E.: An Arctic CCN-limited cloud-aerosol
810 regime, *Atmos. Chem. Phys.*, 11, 165–173, doi:10.5194/acp-11-165-2011, 2011.
811
- 812 Modini, R.L., Frossard, A.A., Ahlm, L., Russell, L.M., Corrigan, C.E., Roberts, G.C., Hawkins,
813 L.N., Schroder, J.C., Bertram, A.K. Zhao, R., Lee, A.K.Y., Abbatt, J.P.D., Lin, J., Nenes, A.,
814 Wang, Z., Wonaschütz, A., Sorooshian, A., Noone, K.J., Jonsson, H., Seinfeld, J.H.,
815 Toom-Sauntry, D., Macdonald, A.M., and Leaitch W.R.: Primary marine aerosol-cloud
816 interactions off the coast of California, *J. Geophys. Res. Atmos.*, 120, 4282–4303,
817 doi:10.1002/2014JD022963, 2015.
818
- 819 Morrison, H., de Boer, G., Feingold, G., Harrington, J., Shupe, M.D., and Sulia K.: Resilience of
820 persistent Arctic mixed-phase clouds, *Nat. Geosci.*, 5, 11–17, doi:10.1038/ngeo1332, 2012.
821
- 822 Najafi, M. R., Zwiers, F.W. and Gillett N.P.: Attribution of Arctic temperature change to
823 greenhouse-gas and aerosol influences. *Nature Climate Change*, doi: 10.1038/NCLIMATE2524,
824 2015.
825
- 826 Peng, Y., Lohmann, U., and Leaitch, R.: The cloud optical depth – cloud droplet effective radius
827 relationship for clean and polluted clouds from RACE and FIRE.ACE. *J. Geophys. Res.*, 107,
828 4106, 10.1029/2000JD000281, 2002.
829
- 830 Penner J.E., Quaas, J., Storelvmo, T., Takemura, T., Boucher, O., Guo, H., Kirkevåg, A.,
831 Kristjánsson, J.E., and Seland, Ø.: Model intercomparison of indirect aerosol effects, *Atmos.*
832 *Chem. Phys.*, 6, 3391–3405. doi:10.5194/acp-6-3391-2006, 2006.
833



- 834 Quinn, P.K., Bates, T.S., Baum, E., Doubleday, N., Fiore, A.M., Flanner, M., Fridlind, A.,
835 Garrett, T.J., Koch, D., Menon, S., Shindell, D., Stohl, A., and Warren S.G.: Short-lived
836 pollutants in the Arctic: Their climate impact and possible mitigation strategies, *Atmos. Chem.*
837 *Phys.*, 8, 1723–1735, doi:10.5194/acp-8-1723-2008, 2008.
- 838
839 Rosenfeld, D., Rudich, Y., and Lahav, R.: Desert dust suppressing precipitation: A possible
840 desertification feedback loop, *Proc. Natl. Acad. Sciences*, 98, 5975–5980, 2001.
- 841
842 Sandvik, A., Biryulina, M., Kvamsto, N., Stamnes, J., and Stamnes, K.: Observed and simulated
843 microphysical composition of Arctic clouds: Data properties and model validation, *J. Geophys.*
844 *Res.*, 112, D05205, doi:10.1029/2006JD007351, 2007.
- 845
846 Shindell, D.T., Chin, M., Dentener, F., Doherty, R.M., Faluvegi, G., Fiore, A.M., Hess, P., Koch,
847 D.M., MacKenzie, I.A., Sanderson, M.G., Schultz, M.G., Schulz, M., Stevenson, D.S., Teich, H.,
848 Textor, C., Wild, O., Bergmann, D.J., Bey, I., Bian, H., Cuvelier, C., Duncan, B.N., Folberth, G.,
849 Horowitz, L.W., Jonson, J., Kaminski, J.W., Marmer, E., Park, R., Pringle, K.J., Schroeder, S.,
850 Szopa, S., Takemura, T., Zeng, G., Keating, T.J., and Zuber, A.: A multi-model assessment of
851 pollution transport to the Arctic, *Atmos. Chem. Phys.*, 8, 5353–5372, doi:10.5194/acp-8-5353-
852 2008, 2008.
- 853
854 Shupe, M.D., Kollias, P., Matrosov, S.Y., and Schneider, T.L.: Deriving mixed-phase cloud
855 properties from Doppler radar spectra, *J. Atmos. Ocean. Technol.*, 21, 660–670, 2004.
- 856
857 Shupe, M.D., Persson, P.O.G., Brooks, I.M., Tjernström, M., Sedlar, J., Mauritsen, T., Sjogren,
858 S., and Leck, C.: Cloud and boundary layer interactions over the Arctic sea ice in late summer,
859 *Atmos. Chem. Phys.*, 13, 9379–9400, doi:10.5194/acp-13-9379-2013, 2013.
- 860
861 Stohl A.: Characteristics of atmospheric transport into the Arctic troposphere, *J. Geophys. Res.*,
862 111, D11306, doi:10.1029/2005JD006888, 2006.
- 863
864 Stohl, A., Klimont, Z., Eckhardt, S., Kupiainen, K., Shevchenko, V.P., Kopeikin, V.M., and
865 Novigatsky, A.N.: Black carbon in the Arctic: the underestimated role of gas flaring and
866 residential combustion emissions, *Atmos. Chem. Phys.*, 13, 8833–8855, doi:10.5194/acp-13-
867 8833-2013, 2013.
- 868
869 Ström, J., Umegård, J., Tørseth, K., Tunved, P., Hansson, H.-C., Holmér, K., Wismann, V.,
870 Herber, A., König-Langlo, G.: One year of particle size distribution and aerosol chemical
871 composition measurements at the Zeppelin Station, Svalbard, March 2000–March 2001, *Physics*
872 *and Chemistry of the Earth* 28 (2003) 1181–1190, 2003.
- 873
874 Tjernström, M., Leck, C., Persson, P.O.G., Jensen, M.L., Oncley, S.P., and Targino, A.: The
875 summertime Arctic atmosphere: Meteorological measurements during the Arctic Ocean
876 experiment 2001 (AOE-2001), *B. Am. Meteor. Soc.*, 85, 1305–1321, 2004, 2004.
- 877
878



- 879 Tjernström, M., Leck, C., Birch, C.E., Bottenheim, J.W., Brooks, B.J., Brooks, I.M., Bäcklin, L.,
880 Chang, R.Y.-W., de Leeuw, G., Di Liberto, L., de la Rosa, S., Granath, E., Graus, M., Hansel,
881 A., Heintzenberg, J., Held, A., Hind, A., Johnston, P., Knulst, J., Martin, M., Matrai, P.A.,
882 Mauritsen, T., Müller, M., Norris, S.J., Orellana, M.V., Orsini, D.A., Paatero, J., Persson,
883 P.O.G., Q. Gao, Rauschenberg, C., Ristovski, Z., Sedlar, J., Shupe, M.D., Sierau, B., Sirevaag,
884 A., Sjogren, S., Stetzer, O., Swietlicki, E., Szczodrak, M., Vaattovaara, P., Wahlberg, N.,
885 Westberg, M., and Wheeler, C.R.: The Arctic summer cloud ocean study (ASCOS): Overview
886 and experimental design, *Atmos. Chem. Phys.*, 14, 2823–2869, doi:10.5194/acp-14-2823-2014,
887 2014.
- 888
- 889 Tunved, P., Ström, J., Krejci R.: Arctic aerosol life cycle: linking aerosol size distributions
890 observed between 2000 and 2010 with air mass transport and precipitation at Zeppelin station,
891 Ny-Alesund, Svalbard, *Atmos. Chem. Phys.*, 13, 3643-3660, doi:10.5194/acp-13-3643-2013,
892 2013.
- 893
- 894 United Nations Environment Programme, Near-term Climate Protection and Clean Air Benefits:
895 Actions for Controlling Short-Lived Climate Forcers, UNEP, Nairobi, Kenya,
896 <http://www.unep.org/publications/ebooks/SLCF/>, 2011.
- 897
- 898 Yum, S.S., and Hudson, J.G.: Vertical distributions of cloud condensation nuclei spectra over the
899 springtime Arctic Ocean, *J. Geophys. Res.*, 106, 15045–15052, doi:10.1029/2000JD900357,
900 2001.
- 901
- 902 Zamora, L.M., Kahn, R.A., Cubison, M.J., Diskin, G.S., Jimenez, J.L., Kondo, Y., McFarquhar,
903 G.M., Nenes, A., Thornhill, K.L., Wisthaler, A., Zelenyuk, A., and Ziemba L.D.: Aircraft-
904 measured indirect cloud effects from biomass burning smoke in the Arctic and subarctic, *Atmos.*
905 *Chem. Phys. Discuss.*, 15, 22823–22887, doi:10.5194/acpd-15-22823-2015, 2015, 2015.
- 906
- 907 Zhao, C. and Garrett, T.J.: Effects of Arctic haze on surface cloud radiative forcing. *Geophys.*
908 *Res. Lett.* 10.1002/2014GL062015, 2015.



909 **Table 1.** Summary of averaged cloud observations with $LWC > 0.01 \text{ g m}^{-3}$ for study periods 1 and
 910 2.

<u>Measurement</u>	Period 1 (July 5-11): 35 samples; 1.2 hours in cloud		Period 2 (July 11-21): 27 samples; 0.4 hours in cloud	
	<u>Mean</u>	<u>Median</u>	<u>Mean</u>	<u>Median</u>
Altitude (m-msl)	920	178	1011	835
Temperature ($^{\circ}\text{C}$)	-1.9	-0.4	+1.2	+2.2
CDNC (STP) (cm^{-3})	75 (85)	93 (91)	73 (83)	52 (55)
LWC (STP) (g m^{-3})	0.12 (0.13)	0.10 (0.12)	0.12 (0.13)	0.12 (0.13)
VMD (μm)	17.2	18.7	15.0	14.5
CCNC (cm^{-3}): 17 P-1; 27 P-2	90	120	81	43
N50 (cm^{-3})	113	134	126	68
N100 (cm^{-3})	35	47	81	31
CDNC(STP)/CCNC	0.75	0.56	1.18	1.22
CDNC(STP)/N50	0.82	0.90	0.73	0.68
CDNC(STP)/N100	2.78	2.63	1.37	1.25
CCNC/N50	0.64	0.63	0.64	0.64
CCNC/N100	1.92	1.79	1.27	1.0
CO (ppbv)	79	80	90	87
LWP (g m^{-2}): 13 P-1; 23 P-2	30	27	22	13



Table 2. Summary of averaged observations got low-altitude (LA) and higher-altitude (HA) clouds.

<u>Measurement</u>	LA (<200m): 24 samples; 0.89 hours in cloud		HA (>200m): 38 samples; 0.72 hours in cloud	
	<u>Mean</u>	<u>Median</u>	<u>Mean</u>	<u>Median</u>
Altitude (m-msl)	129	127	1485	1481
Temperature (°C)	+0.6	+0.2	-1.2	+0.9
CDNC (STP) (cm ⁻³)	31 (30)	11 (10)	101 (118)	91 (101)
LWC (STP) (g m ⁻³)	0.10 (0.10)	0.05 (0.05)	0.13 (0.15)	0.13 (0.15)
VMD (µm)	20.7	20.1	13.4	12.5
CCNC (cm ⁻³); 16 LA; 28 HA	74	24	90	58
N50 (cm ⁻³)	91	11	136	133
N100 (cm ⁻³)	26	4	73	47
CDNC(STP)/CCNC	0.61	0.57	1.2	1.2
CDNC(STP)/N50	0.61	0.44	0.91	0.93
CDNC(STP)/N100	2.3	1.4	2.1	1.9
CCNC/N50	0.66	0.71	0.68	0.64
CCNC/N100	1.8	1.6	1.5	1.1
CO (ppbv)	81	80	86	83



Figure. Captions

Figure 1. Compilation of the flight tracks. All flights originated from Resolute Bay (74°40'48"N 94°52'12"W).

Figure 2. Satellite images from July 5 when LA clouds were sampled over the two polynyas to the north and from July 8 when LA clouds were sampled along Lancaster Sound (July 8). Lancaster Sound is cloud free on July 5 and mostly covered by cloud on July 8. Resolute Bay is marked with a "X". Images are courtesy of NASA Worldview:
<https://earthdata.nasa.gov/labs/worldview/>.

Figure 3. Four examples of profiles through HA clouds. a) Case from July 7 showing CO, CDNC, CCNC and particle number concentrations, where Nx-100, N100 and N5 are for particles sized between "x" nm and 100 nm, >100 nm and >5 nm respectively. b) Case from July 7 showing LWC, VMD, θ_e and temperature, where VMD, θ_e and temperature have been scaled as indicated in the legend. c) As in a), but case from July 17 and without N5. d) As in b), but case from July 17. e) As in a), but case from July 19. f) As in b) but case from July 19. g) As in a) but case from July 20 and without N5. h) as in b), but case from July 20. The CDNC are all referenced to STP, and θ_e is given in degrees Centigrade before scaling.

Figure 4. Time series during the sampling of low (LA) cloud or fog over the polynyas north of Resolute Bay. a) July 5 time series showing CO, CDNC, CCNC and particle number concentrations, where N30-100 is for particles sized between 30 nm and 100 nm and N100 is for particles sized >100 nm. b) July 7 time series showing CO, CDNC and particle number concentrations, where N20-100, N50-100 and N100 are for particles sized between 20 nm and 100 nm, between 50 nm and 100 nm and >100 nm respectively. CCNC measurements are unavailable for this period on July 7. Wind direction and relative position of polynyas are indicated in both panels. CDNC are referenced to STP.

Figure 5. Time series of altitude, CO, N80-100, N90-100, N100, CCNC and CDNC from low cloud (LA) cloud sampling over Lancaster Sound on July 8. The cloud was deeper over the open water of the Sound (see satellite picture in Fig. 2b). Over the ice to the west, the cloud was not as deep and could not be sampled. Segments over water and ice are indicated at the top of the figure.

Figure 6. Profiles down into cloud showing a) θ_e , b) LWC and c) VMDData for periods 17:27-17:29 UT and 17:38-17:39 UT during July 8. d) shows CDNC, N100, CO and CCNC for the 17:27-17:29 UT profile, and e) shows CDNC, N100, CO and CCNC for the 17:38-17:39 UT profile.

Figure 7. The LWC plotted as a function of the CDNC (a) and VMD (b) for the LA (orange) and HA (blue) samples. Linear regressions for each of the LA and HA samples are also plotted, and the coefficients of determination are given in the legends.



Figure 8. As in Fig. 7a, but only for four identified LA cases (July 5, 7, 8 and 11). Linear regressions for each set of samples are also plotted, and the coefficients of determination are given in the legends.

Figure 9. Plots of CDNC versus a) N100 and b) N50. Points are identified between LA (yellow) and HA (blue) samples, and the 1:1 lines are for reference.

Figure 10. a) CDNC plotted versus the CCNC measured at 0.6% supersaturation; points are identified between LA (yellow) and HA (blue) samples, and linear regressions through the origin are shown. b) CCNC plotted versus N50 and N100; power law fits to each are provided for reference.

Figure 11. The mean VMD of all cloud samples plotted versus the CDNC. All CDNC are referenced to the in-situ pressure. The dashed vertical green line represents the “CCN-limited” division discussed by Mauritsen et al (2011) and estimated here as 16 cm^{-3} . The solid black line is another reference showing the relationship between VMD and CDNC for a constant LWC: the study mean LWC of 0.12 g m^{-3} (Table 1). Samples with higher CO ($>90 \text{ ppbv}$) are identified by the open red circles. Also highlighted for the discussion are LA samples from July 5 (red dots) and July 7 (orange dots). The median CDNC are 1.3 cm^{-3} and 7.8 cm^{-3} , for July 5 and 7, respectively; the N50 are 6 cm^{-3} and 8.3 cm^{-3} for July 5 and 7, respectively; the N100 are 3 cm^{-3} and 2.2 cm^{-3} for July 5 and July 7, respectively.

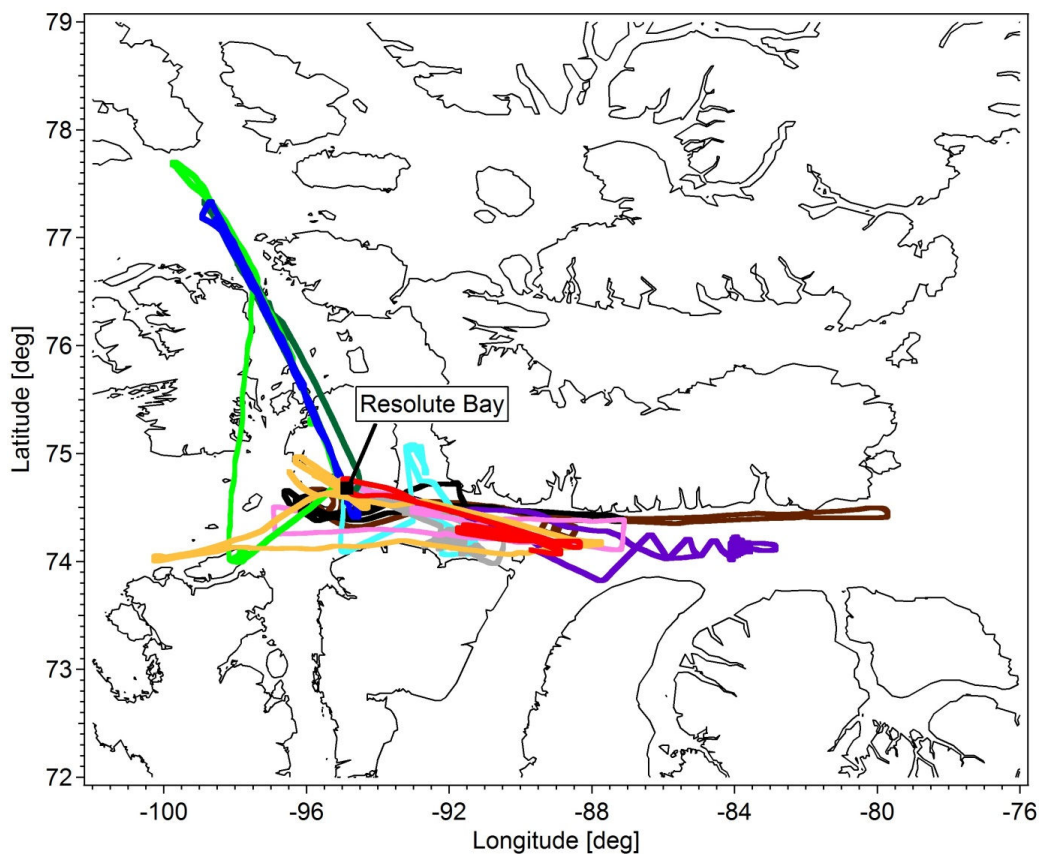


Figure 1. Compilation of the flight tracks. All flights originated from Resolute Bay (74°40'48"N 94°52'12"W).



Figure 2. Satellite images from July 5 when LA clouds were sampled over the two polynyas to the north and from July 8 when LA clouds were sampled along Lancaster Sound (July 8). Lancaster Sound is cloud free on July 5 and mostly covered by cloud on July 8. Resolute Bay is marked with a “X”. Images are courtesy of NASA Worldview:
<https://earthdata.nasa.gov/labs/worldview/>.

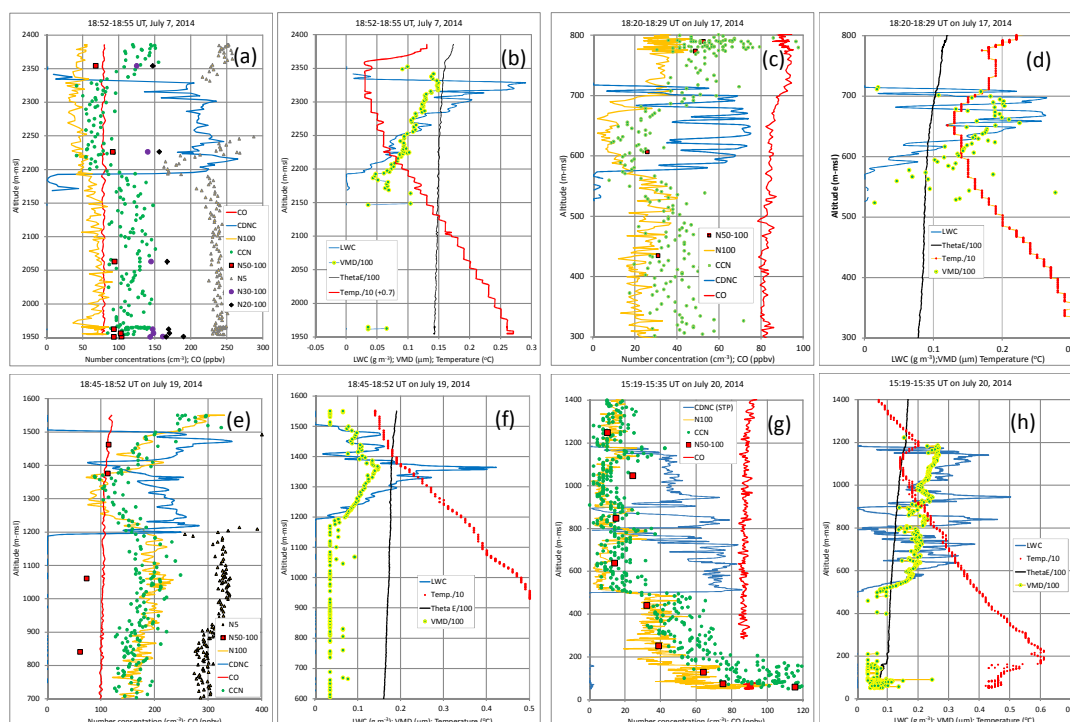


Figure 3. Four examples of profiles through HA clouds. a) Case from July 7 showing CO, CDNC, CCNC and particle number concentrations, where Nx-100, N100 and N5 are for particles sized between “x” nm and 100 nm, >100 nm and >5 nm respectively. b) Case from July 7 showing LWC, VMD, θ_e and temperature, where VMD, θ_e and temperature have been scaled as indicated in the legend. c) As in a), but case from July 17 and without N5. d) As in b), but case from July 17. e) As in a), but case from July 19. f) As in b) but case from July 19. g) As in a) but case from July 20 and without N5. H) as in b), but case from July 20. The CDNC are all referenced to STP, and θ_e is given in degrees Centigrade before scaling.

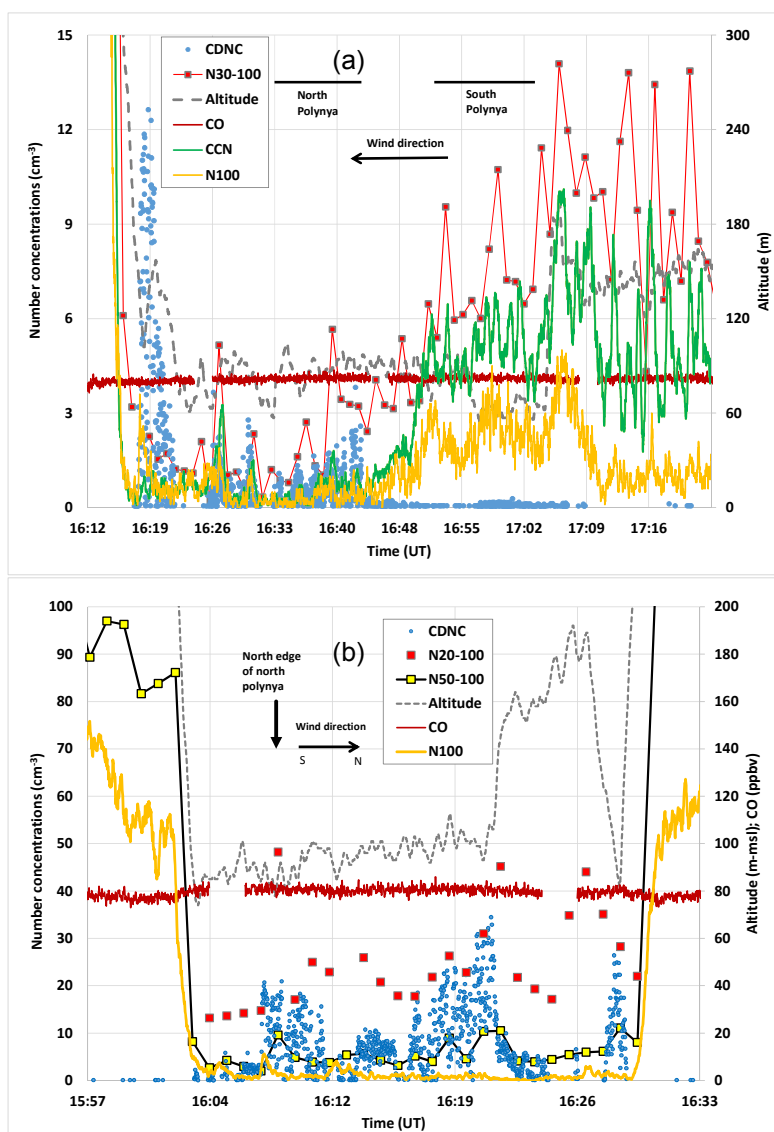


Figure 4. Time series during the sampling of low (LA) cloud or fog over the polynyas north of Resolute Bay. a) July 5 time series showing CO, CDNC, CCNC and particle number concentrations, where N30-100 is for particles sized between 30 nm and 100 nm and N100 is for particles sized >100 nm. b) July 7 time series showing CO, CDNC and particle number concentrations, where N20-100, N50-100 and N100 are for particles sized between 20 nm and 100 nm, between 50 nm and 100 nm and >100 nm respectively. CCNC measurements are unavailable for this period on July 7. Wind direction and relative position of polynyas are indicated in both panels. CDNC are referenced to STP.

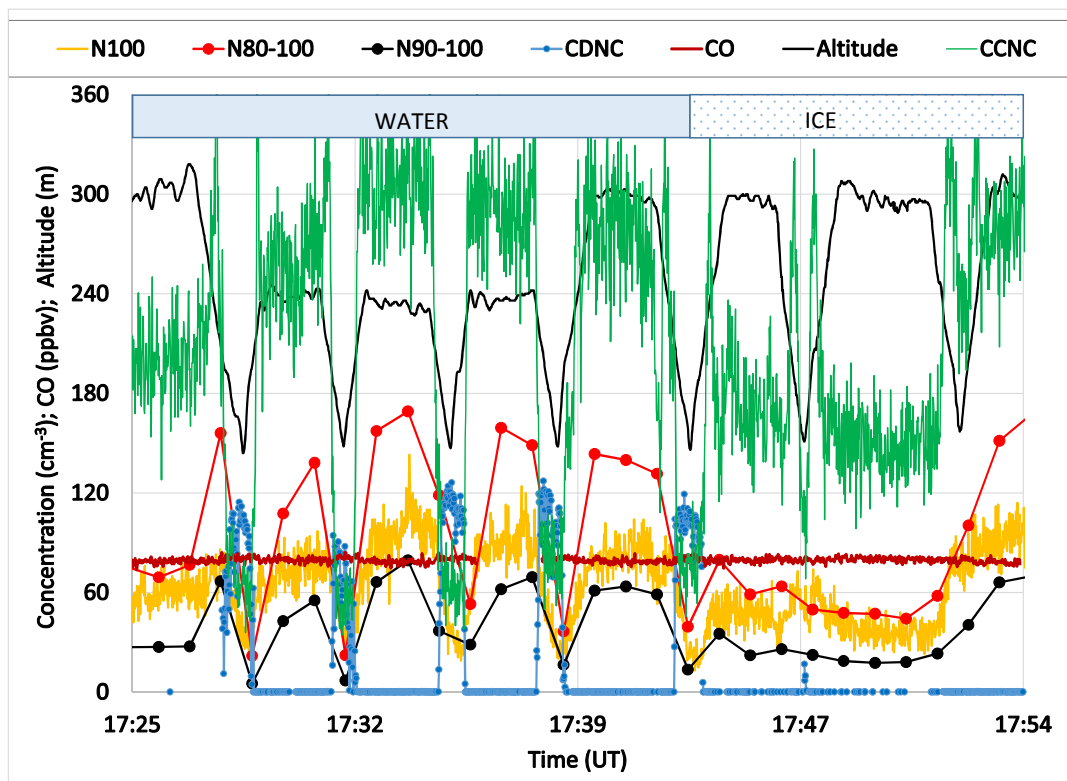


Figure 5. Time series of altitude, CO, N80-100, N90-100, N100, CCNC and CDNC from low cloud (LA) cloud sampling over Lancaster Sound on July 8. The cloud was deeper over the open water of the Sound (see satellite picture in Fig. 2b). Over the ice to the west, the cloud was not as deep and could not be sampled. Segments over water and ice are indicated at the top of the figure.

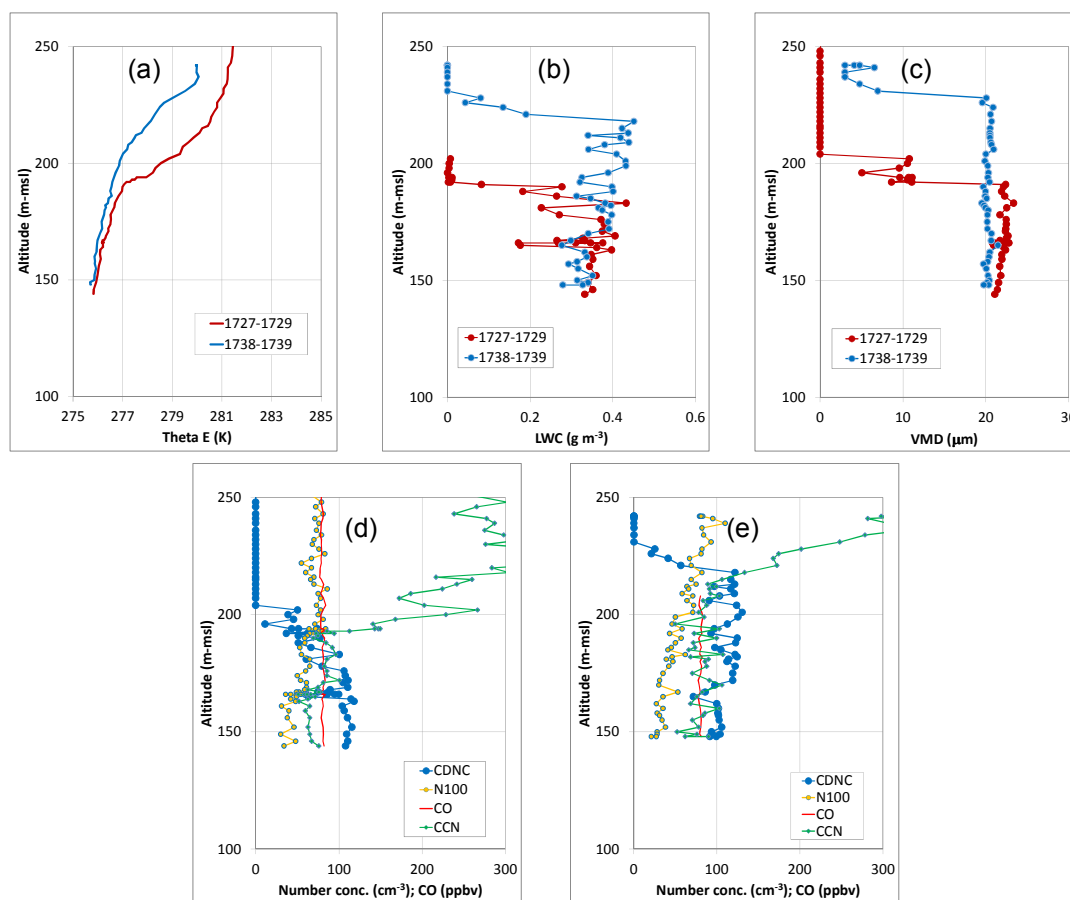


Figure 6. Profiles down into cloud showing a) θ_e , b) LWC and c) VMDData for periods 17:27-17:29 UT and 17:38-17:39 UT during July 8. d) shows CDNC, N100, CO and CCNC for the 17:27-17:29 UT profile, and e) shows CDNC, N100, CO and CCNC for the 17:38-17:39 UT profile.

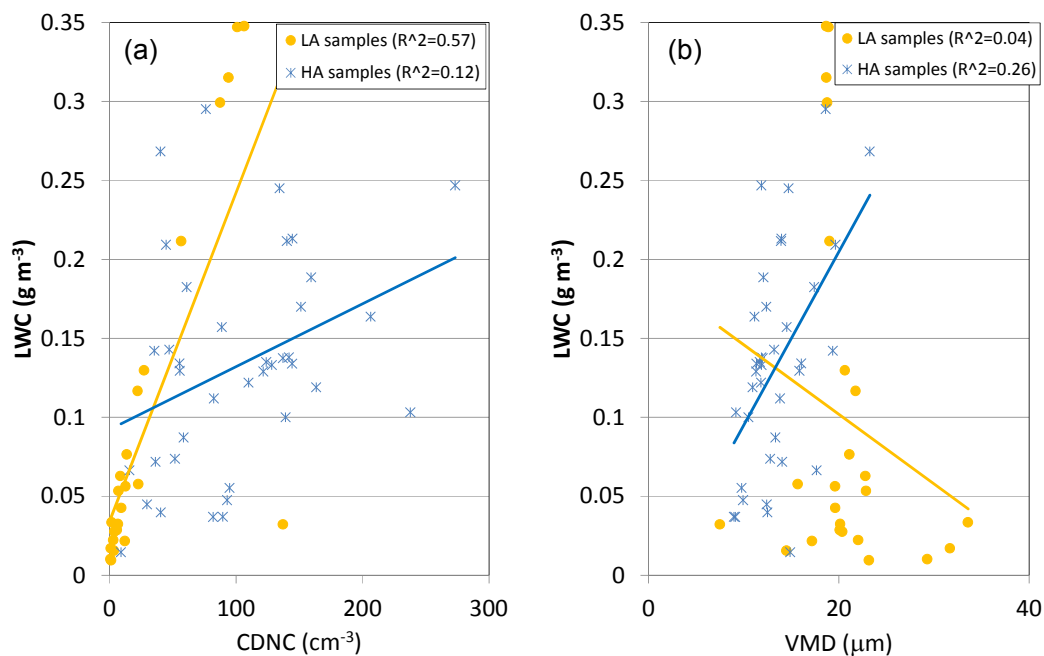


Figure 7. The LWC plotted as a function of the CDNC (a) and VMD (b) for the LA (orange) and HA (blue) samples. Linear regressions for each of the LA and HA samples are also plotted, and the coefficients of determination are given in the legends.

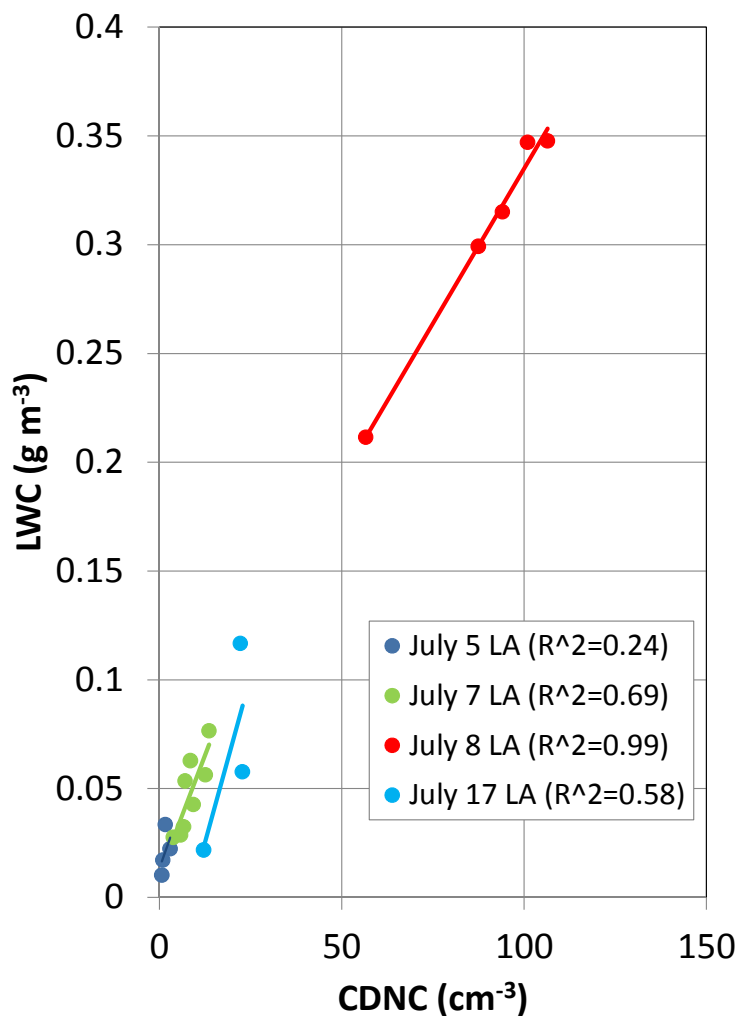


Figure 8. As in Fig. 7a, but only for four identified LA cases (July 5, 7, 8 and 11). Linear regressions for each set of samples are also plotted, and the coefficients of determination are given in the legends.

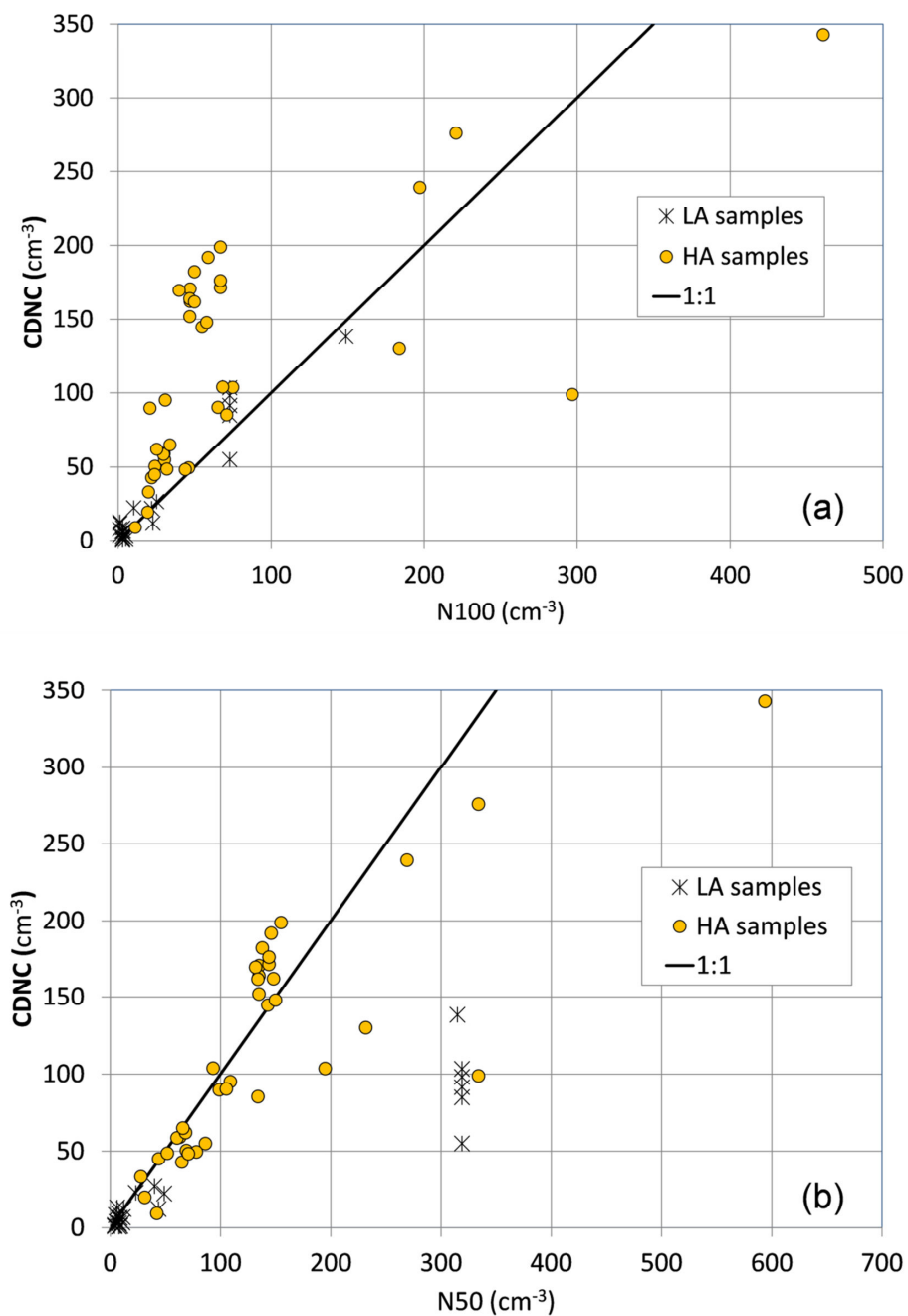


Figure 9. Plots of CDNC versus a) N100 and b) N50. Points are identified between LA (yellow) and HA (blue) samples, and the 1:1 lines are for reference.

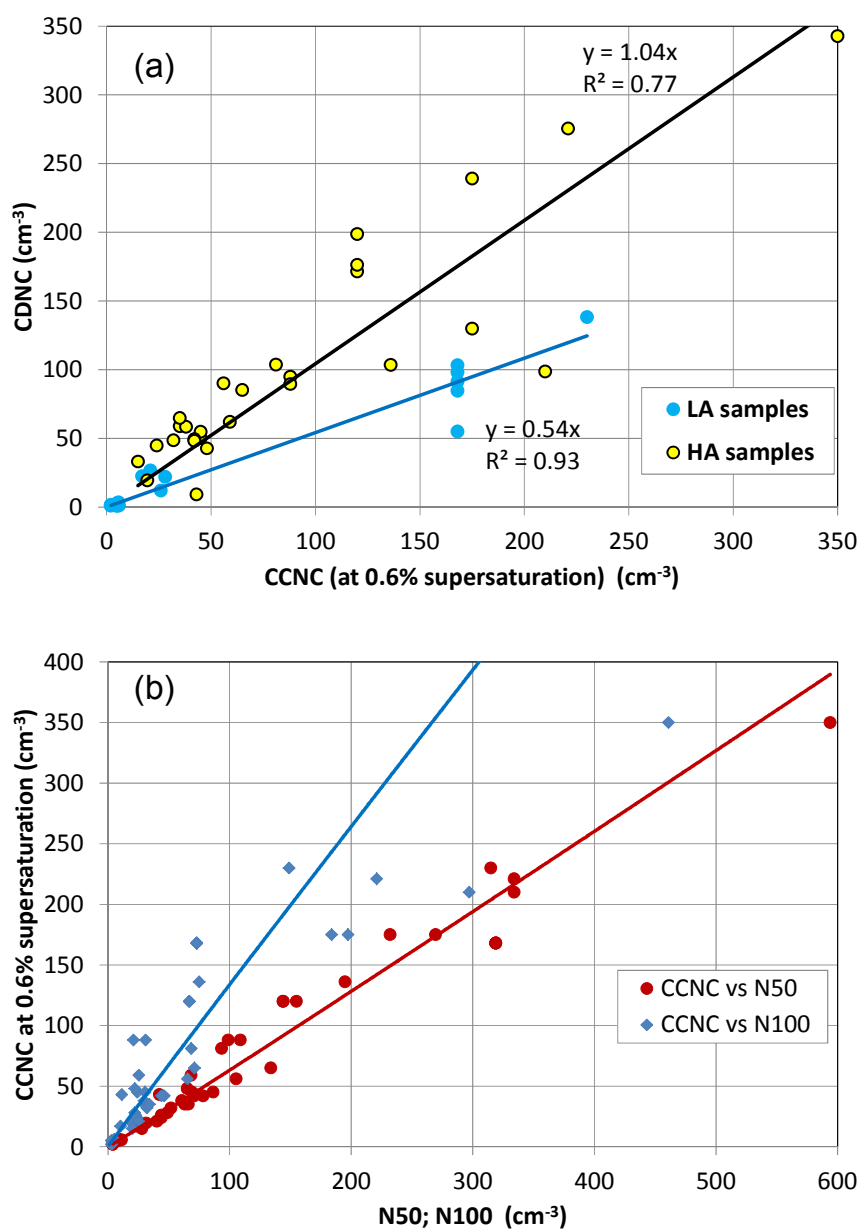


Figure 10. a) CDNC plotted versus the CCNC measured at 0.6% supersaturation; points are identified between LA (yellow) and HA (blue) samples, and linear regressions through the origin are shown. b) CCNC plotted versus N50 and N100; power law fits to each are provided for reference.

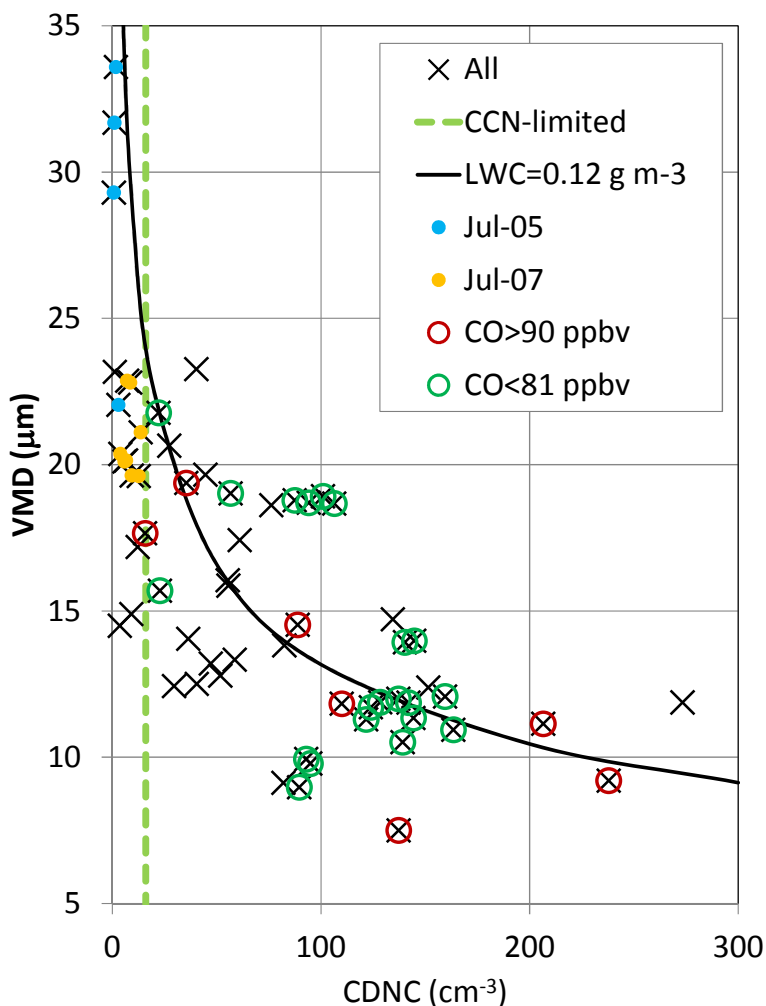


Figure 11. The mean VMD of all cloud samples plotted versus the CDNC. All CDNC are referenced to the in-situ pressure. The dashed vertical green line represents the “CCN-limited” division discussed by Mauritsen et al (2011) and estimated here as 16 cm⁻³. The solid black line is another reference showing the relationship between VMD and CDNC for a constant LWC: the study mean LWC of 0.12 g m⁻³ (Table 1). Samples with higher CO (>90 ppbv) are identified by the open red circles. Also highlighted for the discussion are LA samples from July 5 (red dots) and July 7 (orange dots). The median CDNC are 1.3 cm⁻³ and 7.8 cm⁻³, for July 5 and 7, respectively; the N50 are 6 cm⁻³ and 8.3 cm⁻³ for July 5 and 7, respectively; the N100 are 3 cm⁻³ and 2.2 cm⁻³ for July 5 and July 7, respectively.